

TSPO ligand residence time influences human glioblastoma multiforme cell death/life balance

--Manuscript Draft--

Manuscript Number:	APPT-D-14-00041R2
Full Title:	TSPO ligand residence time influences human glioblastoma multiforme cell death/life balance
Article Type:	Manuscript
Keywords:	Translocator Protein (18 kDa); irreversible TSPO ligand; residence time; Apoptosis; U87MG cells; mitochondrial membrane permeability transition (MPT) pore
Corresponding Author:	Claudia Martini University of Pisa Pisa, ITALY
Corresponding Author Secondary Information:	
Corresponding Author's Institution:	University of Pisa
Corresponding Author's Secondary Institution:	
First Author:	Barbara Costa, PhD
First Author Secondary Information:	
Order of Authors:	Barbara Costa, PhD
	Eleonora Da Pozzo, PhD
	Chiara Giacomelli, PhD
	Sabrina Taliani, PhD
	Sara Bendinelli, PhD
	Elisabetta Barresi, Dr
	Federico Da Settimo, PhD
	Claudia Martini
Order of Authors Secondary Information:	

TSPO ligand residence time influences human glioblastoma multiforme cell death/life balance

1
2
3
4
5
6 Costa Barbara[§], Da Pozzo Eleonora[§], Giacomelli Chiara, Taliani Sabrina, Bendinelli Sara, Barresi
7
8 Elisabetta, Da Settimo Federico, Martini Claudia*.
9

10
11
12
13
14
15 Department of Pharmacy, University of Pisa, via Bonanno, 6-56126 Pisa, Italy.
16
17
18
19
20

21 §: These authors equally contributed to the work.
22
23
24
25
26

27 *: Corresponding authors: Claudia Martini, Department of Pharmacy, University of Pisa, via
28 Bonanno, 6-56126 Pisa, Italy; E-mail address: cmartini@farm.unipi.it. Barbara Costa, Department
29 of Pharmacy, University of Pisa, via Bonanno, 6-56126 Pisa, Italy; E-mail address:
30 bcosta@farm.unipi.it
31
32
33
34
35
36
37
38
39
40
41
42
43
44
45
46
47
48
49
50
51
52
53
54
55
56
57
58
59
60
61
62
63
64
65

Abstract

Ligands addressed to the mitochondrial Translocator Protein (TSPO) have been suggested as cell death/life and steroidogenesis modulators. Thus, TSPO ligands have been proposed as drug candidates in several diseases; nevertheless, a correlation between their binding affinity and *in vitro* efficacy has not been demonstrated yet, questioning the specificity of the observed effects. Since drug-target residence time is an emerging parameter able to influence drug pharmacological features, herein, the interaction between TSPO and irDE-MPIGA, a covalent TSPO ligand, was investigated in order to explore TSPO control on death/life processes in a standardized glioblastoma cell setting. After 90 min irDE-MPIGA cell treatment, 25 nM ligand concentration saturated irreversibly all TSPO binding sites; after 24 h, TSPO *de-novo* synthesis occurred and about 40% TSPO binding sites resulted covalently bound to irDE-MPIGA. During cell culture treatments, several dynamic events were observed: a) early apoptotic markers appeared, such as mitochondrial membrane potential collapse (at 3 h) and externalization of phosphatidylserine (at 6 h); b) cell viability was reduced (at 6 h), without cell cycle arrest. After digitonin-permeabilized cell suspension treatment, a modulation of mitochondrial permeability transition pore was evidenced. Similar effects were elicited by the reversible TSPO ligand PIGA only when applied at micromolar dose. Interestingly, after 6 h, irDE-MPIGA cell exposure restored cell survival parameters. These results highlighted the ligand-target residence time and the cellular setting are crucial parameters that should be taken into account to understand the drug binding affinity and efficacy correlation and, above all, to translate efficiently cellular drug responses from bench to bedside.

Keywords: Translocator Protein (18 kDa); irreversible TSPO ligand; residence time; apoptosis; U87MG cells; mitochondrial membrane permeability transition (MPT) pore.

Introduction

1
2
3 TSPO has been proposed to play a key role in critical cell processes such as cell death/survival,
4
5 differentiation, heme synthesis, porphyrin transport, regulation of mitochondrial function, and
6
7 steroidogenesis [1]. Although TSPO expression is particularly abundant in steroid/neurosteroid
8
9 producing cells, it has been found in every tissue examined, showing abnormal levels in different
10
11 pathological conditions, particularly in cancer and neuroinflammation [1, 2]. All these features have
12
13 led to propose TSPO as a promising pharmacological target and a strategic diagnostic tool. Several
14
15 synthetic ligands with nanomolar/subnanomolar binding affinity to TSPO have been developed [3]
16
17 and some of these are under investigation in Alzheimer's disease [4], multiple sclerosis [5],
18
19 neurotrauma [6], neuroinflammation [7], anxiety disorders [8], cardiovascular diseases [9], and
20
21 cancer [10]. Clinical trials for some TSPO ligands are concluded (Clinical Trials.gov Identifier:
22
23 NCT00108836) or are currently recruiting participants (NCT01547780), and the marketed
24
25 Etifoxine, a TSPO ligand, is already clinically approved for the treatment of anxiety-related
26
27 disorders (Stresam®, Biocodex, Gentilly, France). Concerning the results obtained by the closed
28
29 Phase II study (NCT00108836), the TSPO ligand XBD173 (AC-5316, Emapunil) has shown a
30
31 mean reduction, compared with placebo, in anxiety from baseline to week 6 in patients with
32
33 generalized anxiety disorder.
34
35
36
37
38
39
40
41

42
43 Ligands for TSPO have shown both pro-survival and antiproliferative/pro-apoptotic activities, or
44
45 can act as chemo-sensitizers [11-31]. Classic TSPO ligands have been demonstrated to stimulate
46
47 cell proliferation [11-13], to protect against apoptosis [14-16] and to facilitate apoptosis [17-30].
48
49 However, the effects of these TSPO ligands on cell death/life mechanisms may vary depending on
50
51 the ligand concentration, the experimental setting and the type of cell populations. Interestingly,
52
53 when used at micromolar concentration in several pharmacological studies, a lack of correlation
54
55 between the binding affinity of a TSPO ligand and its *in vitro* effective dose has emerged [17-30,
56
57 32-36]. This discrepancy has often questioned the specificity of the observed effects. Recent studies
58
59
60
61
62
63
64
65

1 have shown that the affinity of a ligand for its target could not directly define its biological action
2 effectiveness that it may instead be related to the ‘drug-target residence time’ [37]. In support, a
3 retrospective assessment of successfully launched drugs has revealed that their favorable effects in
4 patients may be attributed to long lifetime of the binary drug-target complex [38].
5
6
7
8
9

10 All together, these evidences prompted us to investigate the effects caused by a stable occupancy of
11 the TSPO binding sites. For this purpose, nanomolar doses of irDE-MPIGA, a synthetic ligand that
12 covalently binds TSPO [39] (Fig. 1A), were used at different times. Specifically, in this paper our
13 attention was focused on checking irDE-MPIGA effects in cell death/life processes in a cancer *in*
14 *vitro* model (U87MG cells), comparing the results with those obtained using PIGA, a reversible
15 TSPO ligand [40]. In the complex scenario of TSPO ligand death/life modulation, the obtained data
16 confirmed the pharmacological profiles of drugs depend on their concentrations and demonstrated a
17 correlation between ligand effective dose and residence time. Cellular setting standardization was
18 demonstrated useful to obtain indication about the compensatory cell mechanisms and the final
19 response to the drug.
20
21
22
23
24
25
26
27
28
29
30
31
32
33
34
35
36
37
38
39
40
41
42
43
44
45
46
47
48
49
50
51
52
53
54
55
56
57
58
59
60
61
62
63
64
65

Materials and Methods

Materials

The TSPO ligands irDE-MPIGA and PIGA were synthesized essentially as previously reported [39, 40]. The low passage number human U87MG GBM cell line was obtained from the National Institute for Cancer Research of Genoa (Italy) and monitored for DNA profiling. [³H]PK11195 (Specific Activity 84.8 Ci/mmol) was obtained from Perkin-Elmer Life Sciences. Carbonylcyanide-*m*-chlorophenylhydrazone (CCCP), Nonidet P-40 (NP-40), cyclosporin A (CsA), oligomycin and PK11195 were obtained from Sigma–Aldrich, Milano, Italy. Fluorescent dyes, 5,50,6,60-tetrachloro-1,10,3,30-tetraethylbenzimidazolcarbocyanine iodide (JC-1) and Calcium-Green-5N, were obtained from Molecular Probes, Invitrogen, Milano, Italy. The 3-(4,5-dimethylthiazol-2-yl)-5-(3-carboxymethoxyphenyl)-2-(4-sulfophenyl)-2*H*-tetrazolium (MTS) assay kit was from Promega Italia, Milano, Italy. The RNeasy® Mini Kit was from Qiagen, Milano, Italy and the ProtoScript® cDNA Synthesis Kit was obtained from Biolabs, Euroclone, Milano, Italy. The Muse Annexin V and Dead Cell Kit and the Muse cell cycle kit were from Merck KGaA, Darmstadt, Germany. The ATP synthase specific activity microplate assay kit ab109716 was from Abcam, UK. TSPO polyclonal primary antibody (FL-169) sc-20120, TSPO siRNA (human) sc-40821, siRNA dilution buffer sc-29527, siRNA transfection reagent sc-2058, siRNA transfection medium sc-36868 and control siRNA-A sc-37007 were form Santa Cruz Biotechnology (Santa Cruz, CA). All other chemicals were obtained from standard commercial sources.

Experimental setting

1
2
3
4
5
6 *U87MG cells: quantification of TSPO binding sites by [³H]PK11195 binding assays.* A growing
7
8 body of literature demonstrates that the passage number affects cell line's characteristics, such as
9
10 the responses to stimuli [41,42]. Thus, U87MG cells at low passage numbers were used for all
11
12 analyses. The U87MG cells were cultured in RPMI medium supplemented with 10% FBS, 2 mM L-
13
14 glutamine, 100 U/mL penicillin, 100 µg/mL streptomycin and 1% non-essential amino acids at
15
16 37°C in 5% CO₂. The TSPO expression levels in U87MG cells were quantified by radioligand
17
18 binding assays using [³H]PK11195, as previously described [43]. Briefly, aliquots of U87MG cell
19
20 membranes (20 µg of proteins) were incubated in triplicates with increasing [³H]PK11195
21
22 concentrations (0.5-20 nM) in the presence or the absence of unlabeled 1 µM PK11195, in the final
23
24 volume of 500 µl of assay buffer for 90 min at 0°C. The ethanol concentration in the incubation
25
26 buffer was less than 1% and did not interfere with specific [³H]PK11195 binding. Samples were
27
28 rapidly filtered under vacuum through GF/C glass fiber filters. After being washed four times with 3
29
30 ml of assay buffer, radioactivity trapped on the filter was measured by liquid scintillation counter
31
32 (TopCount; PerkinElmer Life and Analytical Sciences; 65% counting efficiency). In U87MG cell
33
34 membranes, [³H]PK11195 maximum number of binding sites (Bmax) and affinity (Kd) were
35
36 determined by Scatchard analysis of saturation binding data. Saturation data were fitted using Prism
37
38 software (version 3.0; GraphPad Software Inc., San Diego, CA).
39
40
41
42
43
44
45
46

47
48 *U87MG cells: drug treatments.* The U87MG cells were seeded and after 24 h, the culture medium
49
50 was replaced with fresh medium containing irDE-MPIGA (solubilized in DMSO) or DMSO
51
52 (control sample). The DMSO did not exceed 1% (v/v). The quantification of Bmax value allowed
53
54 calculating the irDE-MPIGA dose useful to saturate TSPO binding sites and to use for U87MG cell
55
56 treatments. For each experiment, a single irDE-MPIGA dose (1.25×10^{-3} nmol/ 1×10^6 cells) was
57
58 applied to U87MG cell cultures and specific effects exerted by the compound were monitored at
59
60
61
62
63
64
65

1 indicated time points up to 24 h treatment. In parallel, the U87MG cells were treated with the
2 reversible TSPO ligand PIGA.
3

4
5 *U87MG cells: irDE-MPIGA-TSPO stable interaction determination.* irDE-MPIGA- or DMSO-
6 treated U87MG cell membranes (20 µg) were incubated with a single [³H]PK11195 concentration
7 (4 nM) for 90 min at 0°C. Non-specific [³H]PK11195 binding was determined in the presence of
8 1 µM PK11195. After incubation time, the samples were processed as above reported.
9

10
11
12
13
14
15
16 *U87MG cells after treatment: TSPO expression levels determination.* Following U87MG cell
17 treatment with irDE-MPIGA, the relative quantification of TSPO mRNA and protein were
18 performed by real-time reverse transcription polymerase chain reaction (real-time RT-PCR) and
19 Western blot analysis, respectively, as previously described [44, 45].
20
21
22
23
24
25

26 For real-time RT-PCR analysis, total RNA was isolated from DMSO- or irDE-MPIGA-treated
27 U87MG cells using the RNeasy® Mini Kit. The purity of the RNA samples was determined by
28 measuring the absorbance at 260:280 nm. cDNA synthesis was performed with 500 ng of RNA
29 using the Quantitect® reverse transcriptase kit. The primers used for the RT-PCR were designed to
30 span intron/exon boundaries to ensure that products did not include genomic DNA. The nucleotide
31 sequences of primers were: FOR- 5'-CTG GGG CAC GCT CTA CTC-3'; REV 5'-CAG CAG
32 GAG CTC CAC CAA G-3'. The RT-PCR reactions consisted of 12.5 µL of Brilliant® II SYBR®
33 Green premix, 2.5 µL of both the forward and reverse primers (300 nM), 3 µL of cDNA and 4.5 µL
34 of H₂O. All reactions were performed for 40 cycles using the following temperature profiles: 98 °C
35 for 30 seconds; 55 °C for 30 seconds and 72 °C for 3 seconds. β-actin was used as the housekeeping
36 gene. The primers for β-actin mRNA amplification were: FOR: 5'-GCA CTC TTC CAG CCT TCC
37 TTC C-3'; REV-5'-GAG CCG CCG ATC CAC ACG-3'. PCR specificity was determined using
38 both a melting curve analysis and gel electrophoresis, and the data were analyzed by the standard
39 curve method. TSPO mRNA levels for each sample were normalized against β-actin mRNA levels,
40 and relative expression was calculated using the Ct value.
41
42
43
44
45
46
47
48
49
50
51
52
53
54
55
56
57
58
59
60
61
62
63
64
65

1 For Western blot analysis, the 24 h DMSO- or irDE-MPIGA-treated U87MG cells were lysed for
2 60 min at 4 °C by adding RIPA buffer (9.1 mM NaH₂PO₄, 1.7 mM Na₂HPO₄, 150 mM NaCl, pH
3 7.4, 0.5% sodium deoxycholate, 1% Nonidet P-40, 0.1% SDS and a protease inhibitor cocktail).
4 Cell extracts (50 µg) were diluted in Laemmli solution, resolved by SDS-PAGE (8.5%), transferred
5 to PVDF membranes and probed overnight at 4 °C with a primary anti-TSPO antibody (1:200 (FL-
6 169): sc-20120; epitope corresponding to amino acids 1-169, representing TSPO full length of
7 human origin). The primary antibody was detected using anti-rabbit IgG light chains conjugated to
8 peroxidase (diluted 1:10,000). The peroxidase was detected using a chemoluminescent substrate
9 (ECL, Perkin Elmer).
10
11
12
13
14
15
16
17
18
19
20
21
22
23
24

25 U87MG cells after treatment: survival analysis

26
27
28
29
30
31 Cell survival analysis was determined by conventional viability assays [46]. Specifically, cell
32 number was determined using Trypan blue dye exclusion assay and Scepter 2.0 Automated Cell
33 Counter (Millipore) as previously described [47]. The colorimetric assay utilizing MTS reagent was
34 used to establish the PIGA concentration that inhibited 50% (IC₅₀ value) of U87MG cell survival
35 after 24 h of treatment and was performed according to the manufacturer's instructions. Sigmoidal
36 dose-response curves were generated using GraphPad Prism 4 software (GraphPad Software Inc.,
37 San Diego, CA), from which the IC₅₀ value was derived.
38
39
40
41
42
43
44
45
46
47
48
49
50
51
52
53
54
55
56
57
58
59
60
61
62
63
64
65

U87MG cells: irDE-MPIGA specific effect determination

1
2
3
4
5
6 To investigate the specificity of the irDE-MPIGA-induced effects in U87MG cells, cell survival
7
8 analysis was performed in U87MG cells transfected with a siRNA specifically designed for the
9
10 silencing of the human TSPO (sc-40821, Santa Cruz Biotechnology). The siRNA was transfected
11
12 with siRNA transfection reagent (sc-29528) to a final concentration of 50 nM, following the
13
14 manufacturer's protocol. In parallel to each silencing experiment, an ineffective sequence of RNA
15
16 was used as negative control (sc-37007). Transfected U87MG cells were used 48 and 72 h after
17
18 siRNA transfection. The silence efficacy was verified by [³H]PK11195 binding assays. Specifically,
19
20 U87MG cell membrane homogenates (20 µg) were incubated with [³H]PK11195 (6 nM) for 90 min
21
22 at 0°C in the final volume of 500 µl of assay buffer. Non-specific [³H]PK11195 binding was
23
24 determined in the presence of 1 µM PK11195. After incubation time, the samples were processed as
25
26 above reported. For cell survival analysis, transfected U87MG cells were treated with DMSO or a
27
28 nanomolar dose of irDE-MPIGA (1.25×10^{-3} nmol/ 1×10^6 cells) for 6 h and the viable and dead cells
29
30 were determined by Trypan blue dye exclusion assay.
31
32
33
34
35
36
37

38
39 To explore if irDE-MPIGA affected the activity of ATP synthase, the activity and quantity of ATP
40
41 synthase derived by U87MG cells were analyzed using a multiplexing microplate kit (ab109716,
42
43 Abcam, UK), according to the manufacturer's instructions. Briefly, the supplied detergent (10 %
44
45 v/v) was added to the thawed U87MG cell homogenates (5 mg/ml) for obtaining solubilization of
46
47 intact ATP synthase. Then, ATP synthase was immunocaptured within the wells (50 µg
48
49 protein/well) of the microplate and the enzyme activity measured by monitoring the rate of decrease
50
51 in absorbance at 340 nm over time. Subsequently, in these same wells, the quantity of ATP synthase
52
53 was determined by adding an ATP synthase specific antibody conjugated with alkaline phosphatase.
54
55
56
57 The enzyme quantity was monitored as the change in absorbance at 405 nm over time. The
58
59 sensitivity of the assay was monitored by the use of 100 nM oligomycin. To evaluate if TSPO
60
61
62
63
64
65

1 ligand affected ATP synthase activity, the relative ATP synthase specific activity was compared
2 between TSPO ligand-treated and control sample. In parallel, the classic TSPO ligand PK11195
3
4 was used as reference TSPO ligand at 2.5 μ M and 250 μ M.
5
6
7
8
9

10 U87MG cells after treatment: Cell cycle analysis

11
12
13
14
15
16
17 The measurement of the percentage of cells in the G₀/G₁, S, and G₂/M phases of cell cycle was
18 performed using the Muse™ Cell Analyzer (Muse™ Cell Analyzer, Merck KGaA, Darmstadt,
19 Germany). Briefly, treated U87MG cells were collected and centrifuged at 300 x g for 5 minutes.
20 After washing with 1X PBS, cells were fixed, slowly adding 1 mL of ice cold 70% ethanol and
21 maintaining o/n at -20°C. Then, a cell suspension aliquot (containing at least 2 x 10⁵ cells) was
22 centrifuged at 300 x g for 5 minutes, washed once with 1X PBS and suspended in the fluorescent
23 reagent (Muse™ Cell Cycle reagent). After incubation for 30 min, the measurements of the
24 percentage of cells in the phases of cell cycle were acquired.
25
26
27
28
29
30
31
32
33
34
35
36
37
38
39

40 U87MG cells after treatment: mitochondrial potential change analysis

41
42
43
44
45
46
47 Changes in mitochondrial potential ($\Delta\Psi$ m) were assessed using the fluorescent dye JC-1, which has
48 been considered a reliable and sensitive fluorescent probe for detecting differences in $\Delta\Psi$ m [48,
49 49]. JC-1 distributes first into cytoplasm (emitting green fluorescence) and then it is taken into
50 mitochondria, where it forms aggregates (showing orange/red fluorescence) [50]. It has been
51 established that JC1 accumulates within mitochondria in inverse proportion to $\Delta\Psi$ according to the
52 Nernst equation [50] and a reduction of JC-1 orange/red fluorescence is an index of $\Delta\Psi$ dissipation
53
54
55
56
57
58
59
60
61
62
63
64
65

1 [51-53]. The $\Delta\Psi_m$ of treated U87MG cells was determined by labeling both floating and adherent
2 cells with JC-1 for 20 min at room temperature, as previously described [24, 43]. The orange/red
3
4 JC-1 aggregate fluorescence was recorded by flow cytometry in the fluorescence channel 2 (FL-2)
5
6 and green JC-1 monomer fluorescence in the fluorescence channel 1 (FL-1). Necrotic fragments
7
8 were electronically gated out, on the basis of morphological characteristics on the forward light
9
10 scatter versus side light scatter dot plot. As positive control, an aliquot of U87MG cells was
11
12 incubated in the presence of the uncoupling agent CCCP.
13
14
15
16
17
18
19
20

21 U87MG cells after treatment: annexin V/7-AAD staining analysis 22 23 24 25 26

27 The cell apoptosis was measured using Annexin V conjugated to fluorescein-isothiocyanate (FITC)
28
29 and 7-amino-actinomycin (7-AAD) dual staining. Briefly, the treated U87MG cells (both floating
30
31 and adherent cells) were collected and subjected to Annexin V-FITC and 7-AAD staining. Muse™
32
33 Cell Analyzer measured the sample fluorescence of 10,000 cells. In cells undergoing apoptosis,
34
35 Annexin V bound to phosphatidylserine, which translocated from the inner to the outer leaflet of the
36
37 cytoplasmic membrane. Double staining was used to distinguish between viable, early apoptotic, or
38
39 necrotic-late apoptotic cells [54]. Cells that were Annexin V-FITC positive and 7-AAD negative
40
41 were identified as early apoptotic. Cells that were Annexin V-FITC positive and 7-AAD positive
42
43 were identified as cells in late apoptosis or necrotic.
44
45
46
47
48
49
50
51
52
53
54
55
56
57
58
59
60
61
62
63
64
65

U87MG cells after treatment: calcium retention capacity measurement

1
2
3
4
5
6 The Ca^{2+} retention capacity (CRC) was determined as previously described [55] using Calcium
7
8 Green-5N ($\lambda_{\text{ex}}= 505 \text{ nm}$, $\lambda_{\text{em}}= 535 \text{ nm}$), a low affinity membrane-impermeant probe that increases
9
10 its fluorescence emission upon Ca^{2+} binding. U87MG cells were suspended in CRC buffer (250 mM
11
12 sucrose, 1 mM Pi-Tris, and 10 mM MOPS-Tris, pH 7.4) and permeabilized by digitonin (40 μM)
13
14 for 5 min at 0°C . For assays, permeabilized U87MG cell suspensions (2×10^6 cells) were incubated
15
16 with CRC buffer supplemented with the respiratory substrate 5 mM succinate and 0.25 μM Calcium
17
18 Green-5N; Ca^{2+} pulses were added at 3 min intervals until onset of the permeability transition. To
19
20 evaluate the effect exerted by TSPO ligands on MPT pore, CRC was measured by loading
21
22 digitonin-permeabilized cells with a train of Ca^{2+} pulses, in the presence or in the absence of test
23
24 compounds. All experiments were performed at 25°C . By the use of a kinetic program,
25
26 fluorescence was measured with a microplate fluorimeter equipped with thermostatic control (Victor
27
28 Wallac 2, Perkin Elmer, CA, USA).
29
30
31
32
33
34
35
36
37
38

39 Statistical analyses

40
41
42
43
44

45 The nonlinear multipurpose curve-fitting program, GraphPad Prism (version 3.0; GraphPad
46
47 Software Inc., San Diego, CA), was used for data analysis and graphic presentations. All data are
48
49 presented as the means \pm SEM. Statistical analysis was performed by one-way analysis of variance
50
51 (ANOVA) with Bonferroni's corrected t-test for post-hoc pair-wise comparisons. $P < 0.05$ was
52
53 considered statistically significant.
54
55
56
57
58
59
60
61
62
63
64
65

Results

Quantification of TSPO binding sites in human U87MG cells

The U87MG cell line was chosen as *in vitro* cancer model. Previous literature data have demonstrated that this cell line expresses TSPO, but TSPO levels have never been quantified [56]. In the present work, TSPO levels were measured in U87MG cells by radioligand binding assays using the high affinity TSPO radioligand [³H]PK11195, as described in several cellular systems [43, 57]. TSPO density was quantified in terms of maximum specific binding of [³H]PK11195 in membrane homogenate obtained by U87MG cells. The [³H]PK11195 specific binding reached saturation and the Scatchard analysis of saturation data yielded a single straight-line plot indicating the presence of a homogenous population of high affinity binding sites ($K_d = 4.2 \pm 0.4$ nM). The value of maximum number of binding sites (B_{max}) was 3340 ± 40 fmol/mg protein (Fig. 1B). As described in methods section, the B_{max} value was used to calculate the irDE-MPIGA dose useful to saturate TSPO binding sites during U87MG cell treatments.

irDE-MPIGA interacts stably with TSPO during U87MG cell treatment

To determine whether the irDE-MPIGA stably interacted with TSPO following cell treatment, radioligand binding assays were performed on membrane homogenates obtained from U87MG cells treated with TSPO saturating irDE-MPIGA concentration. Specifically, [³H]PK11195 binding assay was explored in U87MG cell membrane homogenates after 1.5 h cell treatment (time required for a covalent irDE-MPIGA-TSPO interaction [39]) and 24 h cell treatment. After cell treatments, it would be expected that [³H]PK11195 did not bind to TSPO binding sites, as they should be already

1 occupied by irDE-MPIGA. This was observed in 1.5 h irDE-MPIGA-treated U87MG cell
2 membrane homogenates (Fig. 2A). In 24 h irDE-MPIGA-treated sample, only a partial abolition of
3 the [³H]PK11195 bond was evidenced, suggesting that only a portion of TSPO binding sites (about
4 40 %) was stably occupied by irDE-MPIGA (Fig. 2A). We hypothesized that the cell treatment with
5 irDE-MPIGA stimulated the *de novo* synthesis of TSPO molecules, which remained “irDE-
6 MPIGA-free” due to unavailability of compound in culture medium. In support of this thesis, real-
7 time RT-PCR analysis showed that TSPO mRNA levels increased after irDE-MPIGA treatment for
8 6 and 12 h (Fig. 2B). In an attempt to evaluate whether the increase of mRNA corresponded to
9 increased TSPO protein levels, Western blotting analysis was performed. Using an antibody
10 directed to human TSPO full length amino acid sequence, the blotting showed a band corresponding
11 to 54 kDa molecular weight (Fig. 2C). This band indicated the presence of TSPO polymers, as
12 previously described [58, 59]. Such polymers are formed by covalent binding between TSPO
13 monomers at the carboxyl terminal [59]. The present results show that TSPO polymers are already
14 evident in control U87MG cells and increase in 24 h irDE-MPIGA-treated U87MG cells with
15 respect to control sample (Fig. 2C).
16
17
18
19
20
21
22
23
24
25
26
27
28
29
30
31
32
33
34
35
36
37
38
39

40 irDE-MPIGA inhibits U87MG cell viability 41 42 43 44 45

46 The effect exerted by irDE-MPIGA (as nanomolar single dose) on U87MG cell viability was
47 monitored over the time. The results showed a significant time-dependent reduction of viable
48 U87MG cells after 6 and 24 h of treatment (Fig. 3A). The percentage of dead cells resulted
49 significantly increased in 6h irDE-MPIGA-treated cell sample. In parallel, the effect of the
50 reversible TSPO ligand PIGA on U87MG cell viability was investigated. In order to establish the
51 PIGA dose for cell viability assays, the compound concentration able to inhibit 50% of U87MG cell
52 viability (IC₅₀ value) was determined after 24 h treatment. PIGA induced a dose-dependent
53
54
55
56
57
58
59
60
61
62
63
64
65

1 inhibition of U87MG cell viability with an IC₅₀ value of 2.5±0.5 μM (data not shown). The U87MG
2 cell treatment with PIGA at IC₅₀ dose at various times did not show a significant reduction of cell
3 viability before 24 h treatment (Fig. 3B).
4
5

6
7 In order to assess the specific irDE-MPIGA efficacy to induce death in U87MG cells, we evaluated
8 its effect on cell viability in TSPO silenced cells in comparison with scramble (negative control). As
9 first step, to quantify the TSPO siRNA efficacy to reduce TSPO expression levels, radioligand
10 binding assays were performed. The specific [³H]PK11195 binding to U87MG cell membranes,
11 prepared from negative control and TSPO siRNA cells, was measured at 48 and 72 h from
12 transfection. As showed in Figure 4A, 48 and 72 h after transfection the specific [³H]PK 11195
13 binding was reduced of 32% and 40% in cells transfected with TSPO siRNA, respectively. Cell
14 viability assays showed that the susceptibility of 48 h and 72 h TSPO siRNA transfected cells to the
15 death-inducing effect of irDE-MPIGA was significantly reduced in comparison to those shown by
16 negative control (Fig. 4B). This difference resulted greater in magnitude in 72 h TSPO silenced
17 sample (Fig. 4B).
18
19
20
21
22
23
24
25
26
27
28
29
30
31
32
33
34
35
36
37

38 Nanomolar dose of irDE-MPIGA does not inhibit ATP synthase activity
39
40
41
42
43

44 We evaluated whether the dose of TSPO ligands used for U87MG cell treatments was able to affect
45 ATP synthase activity. To this aim, ATP synthase was solubilized from U87MG cells and the ATP
46 hydrolysis relative specific activity was measured in the absence and in the presence of nanomolar
47 irDE-MPIGA (25 nM) or micromolar PIGA (2.5 μM) or the classic TSPO ligand PK11195 used as
48 reference compound at 2.5 μM and 250 μM. This last concentration was chosen to verify the
49 response of the enzyme to the TSPO ligand, as previously described in literature [60]. The
50 measurement of the relative ATP hydrolysis specific activity revealed that irDE-MPIGA, PIGA and
51
52
53
54
55
56
57
58
59
60
61
62
63
64
65

1 2.5 μ M PK11195 did not significantly affect ATP synthase activity (Fig. 4C). In the presence of
2 250 μ M PK11195, the relative ATP hydrolysis specific activity was 43% with respect to control
3 sample (Fig. 4C). This result was in agreement with the data reported by Cleary and coworkers
4 [60].
5
6
7
8
9

10 irDE-MPIGA does not block cell cycle in U87MG cells 11 12 13 14 15 16 17 18 19

20 In order to monitor whether the observed cell viability reduction was due to inhibition of cell cycle
21 progression, cell cycle analysis was performed after U87MG cell treatments with irDE-MPIGA
22 nanomolar dose (1.25×10^{-3} nmol/ 1×10^6 cells). Results showed comparable G₁, S and G₂/M phases
23 in irDE-MPIGA-treated and DMSO-treated cells (Fig. 5B), suggesting that the TSPO ligand did not
24 block cell cycle in U87MG cells. Similar results were obtained in samples treated with micromolar
25 dose (2.5 μ M) of the reversible TSPO ligand PIGA (Fig. 5C).
26
27
28
29
30
31
32
33
34
35
36
37

38 irDE-MPIGA induces effectively apoptosis in U87MG cells 39 40 41 42 43 44

45 To investigate whether irDE-MPIGA induced apoptosis, dissipation of $\Delta\Psi_m$ and externalization of
46 phosphatidylserine were evaluated on irDE-MPIGA-treated U87MG cells. Specifically, to monitor
47 $\Delta\Psi_m$ changes flow cytometry analysis using JC-1 on irDE-MPIGA-treated U87MG cells following
48 various incubation times was performed. Representative examples of the flow cytometry analysis
49 are shown in Fig. 6A. The majority of control DMSO-treated cells (99%; control sample) showed
50 high fluorescence emission in both channels and were found in the upper right (UR) quadrant of the
51 plot. The remaining DMSO-treated cells (1 %) showed low fluorescence emission in FL2 and
52
53
54
55
56
57
58
59
60
61
62
63
64
65

1 therefore were found in the lower right (LR) quadrant. Upon irDE-MPIGA treatment, an increase
2 was observed in the percentage of the U87MG cells plotting in the LR quadrant, consistent with
3 $\Delta\Psi_m$ dissipation. In particular, significant changes in $\Delta\Psi_m$ were observed after treatment for 3 and
4 6 h, but not at 12 and 24 h (Fig. 6B). The results obtained by similar experiments performed using a
5 micromolar dose of the reversible TSPO ligand PIGA revealed significant $\Delta\Psi_m$ change at 12 and
6 24 h (Fig 6C).

7
8
9
10
11
12
13
14
15 To monitor externalization of phosphatidylserine flow cytometric analysis using Annexin V/7-AAD
16 dual staining was performed (Fig. 7). Annexin V positive and 7-AAD negative U87MG cells were
17 detected, which indicate cells in the early phase of apoptosis, in samples treated with irDE-MPIGA
18 for 6 h (Fig. 7B). Similar results were obtained in samples treated with the reversible TSPO ligand
19 PIGA for 24 h (Fig. 7C).

20
21
22
23
24
25
26
27
28
29
30
31 irDE-MPIGA modulates mitochondrial permeability transition pore in U87MG cells
32
33
34
35
36

37
38 The ability of irDE-MPIGA to induce mitochondrial permeability transition (MPT) was tested with
39 the sensitive Ca^{2+} retention capacity (CRC) assay, a sensitive measure of the propensity of MPT
40 pore to open. The CRC is a quantitative MPT assay that measures the amount of Ca^{2+} that
41 mitochondria can retain before the release of sequestered Ca^{2+} by induction of MPT. “MPT-
42 inhibitors” and “MPT-inducers” are compounds that increase and decrease the amount of Ca^{2+}
43 required to induce MPT, respectively [61]. Specifically, following treatment of U87MG cells with
44 digitonin, CRC was measured by loading cells with a train of Ca^{2+} pulses, in the presence or in the
45 absence of test compounds, until the fast Ca^{2+} release occurred, marking the MPT onset. Control
46 U87MG cells readily took up Ca^{2+} pulses (Fig. 8A) in a process that was sensitive to the uncoupling
47 agent CCCP, suggesting that the Ca^{2+} was loaded specifically into mitochondria (Fig. 8A). In
48
49
50
51
52
53
54
55
56
57
58
59
60
61
62
63
64
65

1 addition, we examined whether CRC was affected by the cyclosporin A (CsA), a well-known
2 inhibitor of MPT pore opening. The results showed that CsA increased CRC, suggesting the drug
3 ability to desensitize the MPT pore to Ca^{2+} in U87MG cells (Fig. 8A). We next tested the effect of
4 TSPO ligands on the CRC. Two typologies of results were obtained depending on the time
5 exposure of U87MG cells with irDE-MPIGA. CRC assay is usually performed with short-time drug
6 exposure (a few minute) before or simultaneously to Ca^{2+} loading. In this experimental setting,
7 irDE-MPIGA interaction with TSPO is still reversible. Therefore, we decided to perform CRC
8 assay both simultaneously to Ca^{2+} loading and after 2 h exposure with irDE-MPIGA before Ca^{2+}
9 loading, which is the time required for the formation of covalent binding [39]. Interestingly, when
10 the irDE-MPIGA low nanomolar dose was simultaneously added to Ca^{2+} loading in cell suspension,
11 the CRC was increased with respect to control sample, indicating that irDE-MPIGA was able to
12 desensitize mitochondria to Ca^{2+} -induced MPT (Fig. 8B). An opposite result was obtained when a
13 low nanomolar dose of irDE-MPIGA was added 2 h before the Ca^{2+} loading. In this experimental
14 condition, the CRC was lowered with respect to control sample, indicating that irDE-MPIGA was
15 able to sensitize mitochondria to Ca^{2+} -induced MPT (Fig. 8C). This ligand-mediated effect on CRC
16 was CsA-sensitive (data not shown). The reversible TSPO ligand PIGA, added at micromolar dose
17 simultaneously to Ca^{2+} loading, lowered CRC with respect to control sample (Fig. 8B).

Discussion

1
2
3
4
5
6 In the present work, the most relevant result concerns the demonstration that several dynamic
7
8 events occurred in human glioblastoma multiforme U87MG cells following the treatment with the
9
10 irreversible TSPO ligand irDE-MPIGA.
11

12
13 The irDE-MPIGA ligand is structurally related to 2-phenylindol-3-ylglyoxylamide specific TSPO
14
15 ligands developed by our group [40], and it has been previously investigated in detail,
16
17 demonstrating the irreversible covalent nature of its interaction with the target protein [39]. A
18
19 number of irreversible TSPO ligands have been previously employed to improve the understanding
20
21 of TSPO structure and ligand binding sites [62-66]. However, to the best of our knowledge, this is
22
23 the first study in which an irreversible ligand was used to investigate a functional activity of TSPO.
24
25
26
27

28
29 After irDE-MPIGA U87MG cell exposure for 3-6 h, a period of time in which the irreversible
30
31 binding occurred, a TSPO saturating nanomolar dose (1.25×10^{-3} nmol/ 1×10^6 cells) was able to
32
33 induce $\Delta\Psi_m$ collapse and externalization of phosphatidylserine, all events characteristic of early
34
35 apoptotic stages [67,68]. The same cellular responses were evidenced using the reversible TSPO
36
37 ligand PIGA too, but only at micromolar concentration (2.5 μ M) and following 12 h cell exposure.
38
39

40
41 Other TSPO reversible ligands have been reported to exert the same effect at micromolar ligand
42
43 concentration [17-30]. Both irDE-MPIGA and PIGA were effective to halve the number of viable
44
45 U87MG cells after 24 h cell treatment at nanomolar and micromolar concentration, respectively.
46
47

48
49 The results highlighted that a stable ligand-target interaction is essential to improve the efficacy of
50
51 the ligands, as emerged in the recent papers, in which a correlation between the residence time and
52
53 a potentiation of the pharmacological effects has been demonstrated [69-70]. The present results
54
55 challenge to explore in the future the binding kinetic parameters of the reversible TSPO ligands and
56
57 to investigate cellular responses triggered by ligands with different residence times.
58
59
60
61
62
63
64
65

1
2
3
4
5
6
7
8
9
10
11
12
13
14
15
16
17
18
19
20
21
22
23
24
25
26
27
28
29
30
31
32
33
34
35
36
37
38
39
40
41
42
43
44
45
46
47
48
49
50
51
52
53
54
55
56
57
58
59
60
61
62
63
64
65

It is important to underline that the effects elicited by the irreversible ligand were obtained after a single nanomolar compound administration up to 24 h cell treatment. On the other hand, data obtained after 12-24 h cell treatment showed a restoration of cell survival parameters in U87MG cells, as shown by the disappearance of $\Delta\Psi_m$ collapse and the reduction of dead cell number with respect to control. Actually, a TSPO new synthesis was demonstrated and this event could take into account, at least in part, of the restoration of cell survival which could be due to a compensatory cell mechanism [71]. On the other hand, ligand-TSPO interaction could activate other mechanisms, such as neurosteroid new synthesis, thus determining cellular responses able to reverse the death signals. Studies are in progress to explore this issue in a standardized experimental setting. Noteworthy, several conflicting literature data have been reported for TSPO ligands, which could be arisen from troubles in comparing results from different cellular/subcellular settings [36].

Highly debated data in TSPO literature regards the ability of TSPO ligands to modulate MPT pore [72-80]. In the present work, the TSPO ligand modulatory activity on MTP pore functioning was investigated on U87MG cell suspension with digitonin-permeabilized plasmatic membrane at different times. Notably, using nanomolar irDE-MPIGA before the instauration of TSPO irreversible binding (< 90 min cell treatment time), the ligand caused a major resistance to Ca^{2+} -induced MPT pore opening, a phenomenon that generally causes a protection against cell death. Accordingly, the reversible TSPO ligand PIGA at nanomolar concentration was able to induce cell proliferation in serum-free cell culture conditions (data not shown). In line with this finding, a protection against cell death has been previously demonstrated by nanomolar dose of TSPO ligands such as Ro5-4864 (at 30 nM), diazepam (at 47 nM), and flunitrazepam (at 207 nM) [14]; PK11195 and Ro5-4864 (at 10 nM) [15]; SSR180575 and Ro5-4864 (at 100 nM) [16]. On the contrary, following 2 h irDE-MPIGA cell treatment (a time necessary to form TSPO-ligand covalent binding), a nanomolar ligand concentration favored Ca^{2+} -induced MPT pore opening. The same

1 effect was evidenced using PIGA at micromolar concentration (2.5 μ M), accordingly to data
2 obtained using other TSPO reversible ligands [72-74].
3

4
5 The lack of correlation between TSPO ligand binding affinity and *in vitro* efficacy is another of the
6 most recurrently questioned issue. In other drug-target systems, the drug dose causing a functional
7 effect is usually about 100 times the drug binding affinity to its target (expressed in terms of Kd). In
8 the case of the ligand-TSPO system, the efficacy dose of a TSPO ligand is up to 1,000-100,000
9 times its Kd values [17-30, 32-36].
10
11

12
13 For this reason, it has been suggested that other targets may be involved in determining the cellular
14 activities. ATP synthase (a recently suggested structural MPT pore component [81]) has been
15 proposed as an additional target candidate for TSPO ligands [60, 82]. Actually, irDE-MPIGA and
16 PIGA at nanomolar (25 nM) and low-micromolar (2.5 μ M) concentrations, respectively, did not
17 affect ATP synthase functionality. No effect was shown by the classic TSPO ligand PK11195
18 (2.5 μ M) too, according to literature data [60].
19
20
21
22
23
24
25
26
27
28
29
30
31
32
33

34 In order to verify the specific effect of TSPO ligand irDE-MPIGA siRNA technique was used to
35 silence TSPO expression. The reduction of TSPO levels obtained by genetic manipulation protected
36 against the death-inducing activity of irDE-MPIGA, thus indicating the specific role of TSPO in
37 mediating this effect.
38
39
40
41
42
43

44 In conclusion, in the complex scenario of TSPO generated by conflicting pharmacological data, the
45 irreversible ligand irDE-MPIGA has allowed to monitor the occupancy of TSPO sites in a
46 standardized cellular system and to obtain valuable effects at nanomolar concentration (strictly
47 correlated with its binding affinity), differently from the reversible ligand PIGA. The effects were
48 demonstrated to be related to TSPO occupancy.
49
50
51
52
53
54
55
56

57 Thus, irDE-MPIGA emerges as a useful tool to obtain important information about cellular
58 activities generated by the specific interaction with TSPO in U87MG cells. The obtained results
59
60
61
62
63
64
65

confirmed that the pharmacological profiles of drugs depend on their concentrations and demonstrated a correlation between the ligand effective dose and the residence time.

1
2
3
4
5
6
7
8
9
10
11
12
13
14
15
16
17
18
19
20
21
22
23
24
25
26
27
28
29
30
31
32
33
34
35
36
37
38
39
40
41
42
43
44
45
46
47
48
49
50
51
52
53
54
55
56
57
58
59
60
61
62
63
64
65

Acknowledgements Funding for this study was provided by the Italian Ministry of University and Scientific Research (PRIN-prot. 20098SJX4F; PRIN-prot. 2010W7YRLZ_005 and FIRB-prot. RBFR10ZJQT_002).

Conflict of interest The authors declare no conflict of interest

References

1. Batarseh A, Papadopoulos V (2010) Regulation of translocator protein 18 kDa (TSPO) expression in health and diseases states. *Mol Cell Endocrinol* 327:1–12.
2. Costa B, Da Pozzo E, Martini C (2012) Translocator protein as a promising target for novel anxiolytics. *Curr Top Med Chem* 12:270-285.
3. Taliani S, Da Settimo F, Da Pozzo E, Chelli B, Martini C (2009) Translocator protein ligands as promising therapeutic tools for anxiety disorders. *Curr Med Chem* 16:3359-3380.
4. Barron AM, Garcia-Segura LM, Caruso D et al (2013) Ligand for translocator protein reverses pathology in a mouse model of Alzheimer's disease. *J Neurosci* 33:8891–8897.
5. Daugherty DJ, Selvaraj V, Chechneva OV, Liu XB, Pleasure DE, Deng W (2013) A TSPO ligand is protective in a mouse model of multiple sclerosis. *EMBO Mol Med* 5:891–903.
6. Papadopoulos V, Lecanu L (2009) Translocator protein (18 kDa) TSPO: an emerging therapeutic target in neurotrauma. *Exp Neurol* 219:53–57.
7. Girard C, Liu S, Adams D et al (2012) Axonal regeneration and neuroinflammation: roles for the translocator protein 18 kDa. *Neuroendocrinol* 24:71-81.
8. Rupprecht R, Papadopoulos V, Rammes G et al (2010) Translocator protein (18 kDa) (TSPO) as a therapeutic target for neurological and psychiatric disorders. *Nat Rev Drug Discov* 9:971-88.
9. Qi X, Xu J, Wang F, and Xiao J (2012) Translocator Protein (18 kDa): A Promising Therapeutic Target and Diagnostic Tool for Cardiovascular Diseases. *Oxidative Medicine and Cellular Longevity* 2012:162934.
10. Caballero B, Veenman L, Gavish M (2013) Role of mitochondrial translocator protein (18 kDa) on mitochondrial- related cell death processes. *Recent Pat Endocr Metab Immune Drug Discov* 7:86-101.

- 1
2
3
4
5
6
7
8
9
10
11
12
13
14
15
16
17
18
19
20
21
22
23
24
25
26
27
28
29
30
31
32
33
34
35
36
37
38
39
40
41
42
43
44
45
46
47
48
49
50
51
52
53
54
55
56
57
58
59
60
61
62
63
64
65
11. Ikezaki K, Black KL (1990) Stimulation of cell growth and DNA synthesis by peripheral benzodiazepine. *Cancer Lett* 49:115-120.
12. Hardwick M, Fertikh D, Culty M, Li H, Vidic B, Papadopoulos V (1999) Peripheral-type benzodiazepine receptor in human breast cancer: correlation of breast cancer cell aggressive phenotype with PBR expression, nuclear localization, and PBR-mediated cell proliferation and nuclear transport of cholesterol. *Cancer Res* 59:831–842.
13. Akech J, Sinha Roy S, Das SK (2005) Modulation of cholinephosphotransferase activity in breast cancer cell lines by Ro5-4864, a peripheral benzodiazepine receptor agonist. *Biochem Biophys Res Commun* 333:35-41.
14. Bono F, Lamarche I, Prabonnaud V, Le Fur G, Herbert JM (1999) Peripheral benzodiazepine receptor agonists exhibit potent antiapoptotic activities. *Biochem Biophys Res Commun* 265:457-461.
15. Strohmeier R, Roller M, Sanger N, Knecht R, Kuhl H (2002) Knecht R, Kuhl H. Modulation of tamoxifen-induced apoptosis by peripheral benzodiazepine receptor ligands in breast cancer cells. *Biochem Pharmacol* 64:99-107.
16. Leducq N, Bono F, Sulpice T et al (2003) Role of peripheral benzodiazepine receptors in mitochondrial, cellular, and cardiac damage induced by oxidative stress and ischemia-reperfusion. *J Pharmacol Exp Ther* 306:828-837.
17. Okaro AC, Fennell DA, Corbo M, Davidson BR, Cotter FE (2002) PK11195, a mitochondrial benzodiazepine receptor antagonist, reduces apoptosis threshold in Bcl-XL and Mcl-1 expressing human cholangiocarcinoma cells. *Gut* 51:556–561.
18. Decaudin D, Castedo M, Nemati F et al (2002) Peripheral benzodiazepine receptor ligands reverse apoptosis resistance of cancer cells in vitro and in vivo. *Cancer Res* 62:1388–1393.
19. Xia W, Spector S, Hardy L, et al (2000) Tumor selective G2/M cell cycle arrest and apoptosis of epithelial and hematological malignancies by BBL22, a benzazepine PNAS 97:7494-7499.

- 1
2
3
4
5
6
7
8
9
10
11
12
13
14
15
16
17
18
19
20
21
22
23
24
25
26
27
28
29
30
31
32
33
34
35
36
37
38
39
40
41
42
43
44
45
46
47
48
49
50
51
52
53
54
55
56
57
58
59
60
61
62
63
64
65
20. Maaser K, Höpfner M, Jansen A et al (2001) Specific ligands of the peripheral benzodiazepine receptor induce apoptosis and cell cycle arrest in human colorectal cancer cells. *Br J Cancer* 85:1771-1780.
 21. Sutter AP, Maaser K, Höpfner M et al (2002) Specific ligands of the peripheral benzodiazepine receptor induce apoptosis and cell cycle arrest in human esophageal cancer cells. *Int J Cancer* 102:318-327.
 22. Sutter AP, Maaser K, Barthel B, Scherübl H (2003) Ligands of the peripheral benzodiazepine receptor induce apoptosis and cell cycle arrest in oesophageal cancer cells: involvement of the p38MAPK signalling pathway. *Br J Cancer* 89:564-572.
 23. Walter RB, Raden BW, Cronk MR, Bernstein ID, Appelbaum FR, Banker DE (2004) The peripheral benzodiazepine receptor ligand PK11195 overcomes different resistance mechanisms to sensitize AML cells to gemtuzumab ozogamicin. *Blood* 103:4276-4284.
 24. Chelli B, Lena A, Vanacore R et al. (2004) Peripheral benzodiazepine receptor ligands: mitochondrial transmembrane potential depolarization and apoptosis induction in rat C6 glioma cells. *Biochem Pharmacol* 68:125-134.
 25. Chelli B, Rossi L, Da Pozzo E et al. (2005) PIGA (N,N-Di-n-butyl-5-chloro-2-(4-chlorophenyl)indol-3-ylglyoxylamide), a new mitochondrial benzodiazepine-receptor ligand, induces apoptosis in C6 glioma cells. *Chembiochem* 6:1082-1088.
 26. Park SY, Cho N, Chang I et al (2005) Effect of PK11195, a peripheral benzodiazepine receptor agonist, on insulinoma cell death and insulin secretion. *Apoptosis* 10:537-544.
 27. Jordà EG, Jiménez A, Verdaguer E et al (2005) Evidence in favour of a role for peripheral-type benzodiazepine receptor ligands in amplification of neuronal apoptosis. *Apoptosis* 10:91-104.
 28. Shoukrun R, Veenman L, Shandalov Y et al (2008) The 18-kDa translocator protein, formerly known as the peripheral-type benzodiazepine receptor, confers proapoptotic and

- antineoplastic effects in a human colorectal cancer cell line. *Pharmacogenet Genomics* 18:977-988.
29. Banker DE, Cooper JJ, Fennell DA, Willman CL, Appelbaum FR, Cotter FE (2002) PK11195, a peripheral benzodiazepine receptor ligand, chemosensitizes acute myeloid leukemia cells to relevant therapeutic agents by more than one mechanism. *Leuk Res.* 26:91-106.
30. Hirsch T, Decaudin D, Susin SA et al (1998) PK11195, a ligand of the mitochondrial benzodiazepine receptor, facilitates the induction of apoptosis and reverses Bcl-2-mediated cytoprotection. *Exp Cell Res.* 241:426-34.
31. Oudard S, Carpentier A, Banu E et al (2003) Phase II study of lonidamine and diazepam in the treatment of recurrent glioblastoma multiforme. *J Neurooncol* 63:81-86.
32. Zisterer DM, Hance N, Campiani G, Garofalo A, Nacci V, Williams DC (1998) Antiproliferative action of pyrrolobenzoxazepine derivatives in cultured cells: absence of correlation with binding to the peripheral-type benzodiazepine binding site. *Biochem Pharmacol* 55:397-403.
33. Gorman AM, O'Beirne GB, Regan CM, Williams DC (1989) Antiproliferative action of benzodiazepines in cultured brain cells is not mediated through the peripheral-type benzodiazepine acceptor. *J Neurochem* 53:849-855.
34. Alexander BE, Roller E, Klotz U (1992) Characterization of peripheral-type benzodiazepine binding sites on human lymphocytes and lymphoma cell lines and their role in cell growth. *Biochem Pharmacol* 44:269-274.
35. Hans G, Wislet-Gendebien S, Lallemand F et al (2005) Peripheral benzodiazepine receptor (PBR) ligand cytotoxicity unrelated to PBR expression. *Biochem Pharmacol* 69:819-830.
36. Scarf AM, Auman KM, Kassiou M (2012) Is there any correlation between binding and functional effects at the translocator protein (TSPO) (18 kDa)? *Curr Mol Med* 12:387-397.

- 1
2
3
4
5
6
7
8
9
10
11
12
13
14
15
16
17
18
19
20
21
22
23
24
25
26
27
28
29
30
31
32
33
34
35
36
37
38
39
40
41
42
43
44
45
46
47
48
49
50
51
52
53
54
55
56
57
58
59
60
61
62
63
64
65
37. Tummino PJ, Copeland RA (2008) Residence time of receptor-ligand complexes and its effect on biological function. *Biochemistry* 47:5481-5492.
 38. Guo D, Hillger JM, IJzerman AP, and Heitman LH (2014) Drug-Target Residence Time—A Case for G Protein-Coupled Receptors. *Medicinal Research Reviews*. 34:856–892.
 39. Taliani S, Da Pozzo E, Bellandi M et al (2010) Novel irreversible fluorescent probes targeting the 18 kDa translocator protein: synthesis and biological characterization. *J Med Chem* 53:4085-4093.
 40. Primofiore G, Da Settimo F, Taliani S et al (2004) N,N-dialkyl-2-phenylindol-3-ylglyoxylamides. A new class of potent and selective ligands at the peripheral benzodiazepine receptor. *J Med Chem* 47:1852-1855.
 41. Chang-Liu CM, Woloschok GE (1997) Effect of passage number on cellular response to DNA-damaging agents: cell survival and gene expression. *Cancer Letters* 26:77-86.
 42. Wenger SL, Senft JR, Sargent LM, Bamezai R, Bairwa N, Grant SG (2004) Comparison of established cell lines at different passages by karyotype and comparative genomic hybridization. *Bioscience Reports* 24:631-639.
 43. Chelli B, Salvetti A, Da Pozzo E et al (2008) PK 11195 differentially affects cell survival in human wild-type and 18 kDa Translocator protein-silenced ADF astrocytoma cells. *J Cell Biochem* 105:712-723.
 44. Vandesompele J, De Paepe A, Speleman F (2002) Elimination of primer-dimer artifacts and genomic coamplification using a two-step SYBR green I real-time RT-PCR. *Anal Biochem* 303:95-98.
 45. Costa B, Salvetti A, Rossi L et al (2006) Peripheral benzodiazepine receptor: characterization in human T-lymphoma Jurkat cells. *Mol Pharmacol* 69:37-44.
 46. Costa B, Bendinelli S, Gabelloni P et al. (2013) Human glioblastoma multiforme: p53 reactivation by a novel MDM2 inhibitor. *PLoS One* 8:e72281.

- 1
2
3
4
5
6
7
8
9
10
11
12
13
14
15
16
17
18
19
20
21
22
23
24
25
26
27
28
29
30
31
32
33
34
35
36
37
38
39
40
41
42
43
44
45
46
47
48
49
50
51
52
53
54
55
56
57
58
59
60
61
62
63
64
65
47. Keats E, Khan ZA (2012) Unique responses of stem cell-derived vascular endothelial and mesenchymal cells to high levels of glucose. *PLoS One* 7:e38752.
48. Smiley ST, Reers M, Mottola-Hartshorn C et al (1991) Intracellular heterogeneity in mitochondrial membrane potentials revealed by a J-aggregate-forming lipophilic cation JC-1. *Proc Natl Acad Sci U S A* 88:3671-3675.
49. Di Lisa F, Blank PS, Colonna R et al (1995) Mitochondrial membrane potential in single living adult rat cardiac myocytes exposed to anoxia or metabolic inhibition. *J Physiol* 486:1-13.
50. Perry SW, Norman JP, Barbieri J, Brown EB, Gelbard HA (2011) Mitochondrial membrane potential probes and the proton gradient: a practical usage guide. *Biotechniques* 50:98-115.
51. Stolarczyk M, Naruszewicz M, Kiss AK (2013) Extracts from *Epilobium* sp. herbs induce apoptosis in human hormone-dependent prostate cancer cells by activating the mitochondrial pathway. *J Pharm Pharmacol* 65:1044-1054.
52. Agarwal C, Singh RP, Agarwal R (2002) Grape seed extract induces apoptotic death of human prostate carcinoma DU145 cells via caspases activation accompanied by dissipation of mitochondrial membrane potential and cytochrome c release. *Carcinogenesis* 23:1869-1876.
53. Cossarizza A, Baccarani-Contri M, Kalashnikova G, Franceschi C (1993) A new method for the cytofluorimetric analysis of mitochondrial membrane potential using the J-aggregate forming lipophilic cation 5,5',6,6'-tetrachloro-1,1',3,3'-tetraethylbenzimidazolcarbocyanine iodide (JC-1). *Biochem Biophys Res Commun* 197:40-45.
54. Fadok VA, Voelker DR, Campbell PA et al (1992) Exposure of phosphatidylserine on the surface of apoptotic lymphocytes triggers specific recognition and removal by macrophages. *J Immunol* 148:2207-2216.

- 1
2
3
4
5
6
7
8
9
10
11
12
13
14
15
16
17
18
19
20
21
22
23
24
25
26
27
28
29
30
31
32
33
34
35
36
37
38
39
40
41
42
43
44
45
46
47
48
49
50
51
52
53
54
55
56
57
58
59
60
61
62
63
64
65
55. Li B, Chauvin C, De Paulis D et al (2012) Inhibition of complex I regulates the mitochondrial permeability transition through a phosphate-sensitive inhibitory site masked by cyclophilin D1. *Biochim Biophys Acta* 1817:1628-1634.
 56. Veenman L, Levin E, Weisinger G et al (2004) Peripheral-type benzodiazepine receptor density and in vitro tumorigenicity of glioma cell lines. *Biochem Pharmacol* 68:689-698.
 57. Giusti L, Costa B, Viacava P et al (2004) Peripheral type benzodiazepine receptor in human parathyroid glands: up-regulation in adenoma. *J Endocrinol Invest* 27:826-831.
 58. Boujrad N, Vidic B, Papadopoulos V (1996) Acute action of choriogonadotropin on Leydig tumor cells: changes in the topography of the mitochondrial peripheral-type benzodiazepine receptor. *Endocrinology* 137:5727-5730.
 59. Delavoie F, Li H, Hardwick M et al (2003) In vivo and in vitro peripheral-type benzodiazepine receptor polymerization: functional significance in drug ligand and cholesterol binding. *Biochemistry* 42:4506-4519.
 60. Cleary J, Johnson KM, Opipari AW Jr, Glick GD (2007) Inhibition of the mitochondrial F1F0-ATPase by ligands of the peripheral benzodiazepine receptor. *Bioorg Med Chem Lett* 17:1667-1670.
 61. Bernardi P (1999) Mitochondrial transport of cations: channels, exchangers, and permeability transition. *Physiol Rev* 79:1127-1155.
 62. Broaddus WC, Bennett JP Jr (1990) Peripheral-type benzodiazepine receptors in human glioblastomas: pharmacologic characterization and photoaffinity labeling of ligand recognition site. *Brain Res* 518:199-208.
 63. Lueddens HW, Newman AH, Rice KC, Skolnick P (1986) AHN 086: an irreversible ligand of "peripheral" benzodiazepine receptors. *Mol Pharmacol* 29:540-545.
 64. Newman AH, Lueddens HW, Skolnick P, Rice KC (1987) Novel irreversible ligands specific for "peripheral" type benzodiazepine receptors: (+/-)-, (+)-, and (-)-1-(2-chlorophenyl)-N-(1-methylpropyl)-N-(2-isothiocyanatoethyl)-3-isoquinolinecarboxamide

- and 1-(2-isothiocyanatoethyl)-7-chloro-1,3-dihydro-5-(4-chlorophenyl)-2H-1,4-benzodiazepin-2-one. *J Med Chem* 30:1901-1905.
65. McCabe RT, Schoenheimer JA, Skolnick P, Newman AH, Rice KC, Reig JA, Klein DC (1989) [3H]AHN 086 acylates peripheral benzodiazepine receptors in the rat pineal gland. *FEBS Lett* 244:263-267.
66. Alenfall J, Batra S (1996) Photoaffinity labeling of peripheral benzodiazepine receptors in R-3327 Dunning prostatic tumors. *Biochem Pharmacol* 51:1009-1013.
67. van Engeland M, Nieland LJ, Ramaekers FC et al (1998) Annexin V-affinity assay: a review on an apoptosis detection system based on phosphatidylserine exposure. *Cytometry* 31:1-9.
68. Galluzzi L, Zamzami N, de La Motte Rouge T, Lemaire C, Brenner C, Kroemer G (2007) Methods for the assessment of mitochondrial membrane permeabilization in apoptosis. *Apoptosis* 12:803-813.
69. Copeland RA, Pompliano DL, Meek TD (2006) Drug-target residence time and its implications for lead optimization. *Nat Rev Drug Discov* 5:730-739.
70. Guo D, Hillger JM, IJzerman AP, Heitman LH (2014) Drug-target residence time-a case for G protein-coupled receptors. *Med Res Rev* 34:856-892.
71. Sutter AP, Maaser K, Gerst B, Krahn A, Zeitz M, Scherübl H (2004) Enhancement of peripheral benzodiazepine receptor ligand-induced apoptosis and cell cycle arrest of esophageal cancer cells by simultaneous inhibition of MAPK/ERK kinase. *Biochem Pharmacol* 67:1701-1710.
72. Sileikyte J, Blachly-Dyson E, Sewell R et al (2014) Regulation of the Mitochondrial Permeability Transition Pore by the Outer Membrane does not Involve the Peripheral Benzodiazepine Receptor (TSPO). *J Biol Chem* 289:13769-13781.
73. Azarashvili T, Baburina Y, Grachev D et al (2014) Carbenoxolone induces permeability transition pore opening in rat mitochondria via the Translocator protein TSPO and connexin43. *Arch Biochem Biophys* 558:87-94.

- 1
2
3
4
5
6
7
8
9
10
11
12
13
14
15
16
17
18
19
20
21
22
23
24
25
26
27
28
29
30
31
32
33
34
35
36
37
38
39
40
41
42
43
44
45
46
47
48
49
50
51
52
53
54
55
56
57
58
59
60
61
62
63
64
65
74. Azarashvili T, Grachev D, Krestinina O et al (2007) The peripheral-type benzodiazepine receptor is involved in control of Ca²⁺-induced permeability transition pore opening in rat brain mitochondria. *Cell Calcium* 42:27-39.
 75. Li J, Wang J, Zeng Y (2007) Peripheral benzodiazepine receptor ligand, PK11195 induces mitochondria cytochrome c release and dissipation of mitochondria potential via induction of mitochondria permeability transition. *Eur J Pharmacol* 560:117-122.
 76. Pastorino JG, Simbula G, Gilfor E, Hoek JB, Farber JL (1994) Protoporphyrin IX, an endogenous ligand of the peripheral benzodiazepine receptor, potentiates induction of the mitochondrial permeability transition and the killing of cultured hepatocytes by rotenone. *J Biol Chem* 269:31041-31046.
 77. Chelli B, Falleni A, Salvetti F, Gremigni V, Lucacchini A, Martini C (2001) Peripheral-type benzodiazepine receptor ligands: mitochondrial permeability transition induction in rat cardiac tissue. *Biochem Pharmacol* 61:695-705.
 78. Kinnally KW, Zorov DB, Antonenko YN, Snyder SH, McEnery MW, Tedeschi H (1993) Mitochondrial benzodiazepine receptor linked to inner membrane ion channels by nanomolar actions of ligands. *Proc Natl Acad Sci U S A*. 90:1374-1378.
 79. Berson A, Descatoire V, Sutton A et al (2001) Toxicity of alpidem, a peripheral benzodiazepine receptor ligand, but not zolpidem, in rat hepatocytes: role of mitochondrial permeability transition and metabolic activation. *J Pharmacol Exp Ther* 299:793-800.
 80. Obame FN, Zini R, Souktani R, Berdeaux A, Morin D (2007) Peripheral benzodiazepine receptor-induced myocardial protection is mediated by inhibition of mitochondrial membrane permeabilization. *Pharmacol Exp Ther* 323:336-345.
 81. Giorgio V, von Stockum S, Antoniel M et al (2013) Dimers of mitochondrial ATP synthase form the permeability transition pore. *Proc Natl Acad Sci USA* 110:5887-5892.

82. Seneviratne MS, Faccenda D, De Biase V, Campanella M (2012) PK11195 inhibits
mitophagy targeting the F1Fo-ATP synthase in Bcl-2 knock-down cells. *Curr Mol Med*
12:476-482.

1
2
3
4
5
6
7
8
9
10
11
12
13
14
15
16
17
18
19
20
21
22
23
24
25
26
27
28
29
30
31
32
33
34
35
36
37
38
39
40
41
42
43
44
45
46
47
48
49
50
51
52
53
54
55
56
57
58
59
60
61
62
63
64
65

Legends

Fig. 1 A) Chemical structure of irDE-MPIGA and schematic representation of its interaction with TSPO. **B)** Representative saturation curve and Scatchard plot (inset) of the specific [³H]PK11195 binding to U87MG cell membranes. U87MG cell membranes were incubated with increasing concentrations of [³H]PK11195 for 90 min at 0 °C. Non-specific binding was determined in the presence of 1 μM PK11195. Data are from a single experiment carried out in triplicate. The K_d and B_{max} values were 4.2 ± 0.4 nM and 3340 ± 40 fmol/mg protein, respectively. Three such experiments yielded similar results.

Fig. 2 U87MG cell treatments with a TSPO saturating nanomolar dose of irDE-MPIGA. **A)** *stable interaction between irDE-MPIGA and TSPO binding sites:* 1.5 or 24 h irDE-MPIGA- (1.25 x 10⁻³ nmol/1x10⁶ cells) or DMSO-treated U87MG cells were used to prepare cell membrane homogenates and perform [³H]PK11195 radioligand binding assays. [³H]PK11195 binding was calculated as fmol/mg of protein and showed as percentage with respect to control. Data are from two experiments carried out in triplicate. A complete inhibition of [³H]PK11195 binding was evidenced in 1.5 h irDE-MPIGA-treated U87MG cell membrane homogenates with respect to control sample (p<0.001). A statistical significant reduction of [³H]PK11195 binding was evidenced in 24 h irDE-MPIGA-treated U87MG cell membrane homogenates with respect to control sample (p<0.01). **B)** *irDE-MPIGA treatment increased TSPO mRNA levels:* irDE-MPIGA- (1.25 x 10⁻³ nmol/1x10⁶ cells) or DMSO-treated U87MG cells for the indicated times were used to perform the relative quantification of TSPO mRNA by real-time RT-PCR. TSPO mRNA levels significantly increased at 6 (p<0.01) and 12 h (p<0.001) of cell treatment. **C)** *irDE-MPIGA treatment increased TSPO polymer levels:* 24 h irDE-MPIGA- (1.25 x 10⁻³ nmol/1x10⁶ cells) or DMSO-treated U87MG cells were used to perform the relative quantification of TSPO protein by Western blot.

1
2
3
4
5
6
7
8
9
10
11
12
13
14
15
16
17
18
19
20
21
22
23
24
25
26
27
28
29
30
31
32
33
34
35
36
37
38
39
40
41
42
43
44
45
46
47
48
49
50
51
52
53
54
55
56
57
58
59
60
61
62
63
64
65

Representative Western blotting chart is presented. TSPO primary polyclonal antibody (FL-169, Santa Cruz Biotechnology) recognizes proteins of approximately 54 kDa in DMSO- and irDE-MPIGA-treated cells, corresponding to TSPO polymers. TSPO polymer levels significantly increased at 24 h of cell treatment ($p < 0.01$).

Fig. 3 irDE-MPIGA inhibits viability of U87MG cells. **A)** *irDE-MPIGA effect on U87MG cell viability.* U87MG cells were treated with irDE-MPIGA nanomolar dose (1.25×10^{-3} nmol/ 1×10^6 cells) or DMSO for indicated times. The graph shows the number of viable and dead cells (mean values \pm SEM). A significant reduction of viable and U87MG cells was evidenced in 6 ($p < 0.01$) and 24 h ($p < 0.001$) irDE-MPIGA-treated sample. A significant increase of cell death were evidenced in 6 h irDE-MPIGA-treated sample ($p < 0.01$). **B)** U87MG cells were treated with a micromolar dose of the reversible TSPO ligand PIGA (2.5 μ M) or DMSO for indicated times. A reduction in U87MG cell viability ($p < 0.001$) and an increase of cell death ($p < 0.001$) were evidenced in 24 h PIGA-treated sample. Bars represent the means of three independent experiments performed in triplicate.

Fig.4 TSPO silencing protects U87MG cells against irDE-MPIGA-induced cell death; and irDE-MPIGA doesn't affect functionality of ATP synthase. **A)** *Assessment of TSPO silencing in U87MG cells by radioligand binding assays.* The specific [3 H]PK11195 binding to scramble (negative control) and TSPO siRNA U87MG cell membranes were determined. The results are expressed as percentage of the specific [3 H]PK11195 binding measured in TSPO siRNA vs negative control cells at which the arbitrary value of 100% was attributed. Data are obtained from at least three independent experiments, done in duplicate. Each bar represents the mean value \pm SEM. The [3 H]PK11195 binding in TSPO silenced cells was significantly reduced 48 h and 72 h after transfection ($***p < 0.001$). **B)** *Effect of TSPO silencing on U87MG cell death induction by irDE-*

1
2
3
4
5
6
7
8
9
10
11
12
13
14
15
16
17
18
19
20
21
22
23
24
25
26
27
28
29
30
31
32
33
34
35
36
37
38
39
40
41
42
43
44
45
46
47
48
49
50
51
52
53
54
55
56
57
58
59
60
61
62
63
64
65

MPIGA. U87MG cells transfected with TSPO siRNA or scramble (negative control) for 48 and 72 h were treated with DMSO or a nanomolar dose of irDE-MPIGA (1.25×10^{-3} nmol/ 1×10^6 cells) for 6 h and then the viable and dead cells were determined by Trypan blue dye exclusion assay. For each sample, the dead cells were expressed as percentage *versus* total cells. The cell death in the irDE-MPIGA-treated cells are scaled in respect to their DMSO controls. In transfected U87MG cells expressing normal TSPO levels (scramble samples), irDE-MPIGA increased cell death approximately 2-fold compared to baseline level (Ctrl-DMSO). In transfected U87MG cells expressing reduced TSPO levels (TSPO siRNA samples), the cell death-inducing effect of irDE-MPIGA was significantly reduced. The results are shown as mean \pm SEM, derived from three independent experiment, done in duplicate. * $p < 0.05$; ** $p < 0.01$. **C)** *irDE-MPIGA effect on ATP synthase functionality*. ATP synthase was solubilized from U87MG cells and the ATP hydrolysis relative specific activity was measured as described in methods section. To evaluate if TSPO ligand affected ATP synthase activity, the relative ATP synthase specific activity was compared between TSPO ligand-treated and control sample. The results showed that both irDE-MPIGA (25 nM) and PIGA (2.5 μ M) did not significantly affect ATP synthase activity. The graph shows also the result obtained by the classic TSPO ligand PK11195 (250 μ M) that was used as reference TSPO compound ($p < 0.05$).

Fig.5 irDE-MPIGA did not block U87MG cell cycle. The percentage of U87MG cell cycle phases was measured after irDE-MPIGA treatment (1.25×10^{-3} nmol/ 1×10^6 cells) for 24 h. **A)** Representative dot plots of cell population profile and DNA content are shown. Histograms represent the results obtained with the Muse™ Cell Cycle software module: they show that the percentage of U87MG cells in each population did not differ between irDE-MPIGA-treated and control cells **(B)** and between micromolar PIGA-treated (2.5 μ M) and control cells **(C)**.

1
2
3
4
5
6
7
8
9
10
11
12
13
14
15
16
17
18
19
20
21
22
23
24
25
26
27
28
29
30
31
32
33
34
35
36
37
38
39
40
41
42
43
44
45
46
47
48
49
50
51
52
53
54
55
56
57
58
59
60
61
62
63
64
65

Fig. 6 nanomolar irDE-MPIGA induces $\Delta\Psi_m$ dissipation in U87MG cells. U87MG cells were treated with nanomolar irDE-MPIGA (1.25×10^{-3} nmol/ 1×10^6 cells) or micromolar PIGA (2.5 μ M) for indicated times. **A)** Representative dot plots of DMSO-treated, or irDE-MPIGA-treated U87MG cells (CCCP is the positive control): after cell treatment with irDE-MPIGA, mitochondrial depolarization is visible by a fluorescence decrease in the FL-2 channel and an increase in FL-1 channel. **B)** Time-course analysis of $\Delta\Psi_m$ in irDE-MPIGA-treated U87MG cells is represented. Histograms show the mean values of U87MG cell percentages either in the UR (polarized mitochondria) or LR (depolarized mitochondria) quadrant of the $\Delta\Psi_m$ analysis plots, derived from three independent experiments. Following U87MG cell exposure to irDE-MPIGA for different periods of time, a progressive time-dependent changes of $\Delta\Psi_m$ values was revealed, indicating that irDE-MPIGA was able to induce $\Delta\Psi_m$ dissipation in U87MG cells ($p < 0.001$). **C)** Time-course analysis of $\Delta\Psi_m$ in PIGA-treated U87MG cells is represented. PIGA induced $\Delta\Psi_m$ dissipation after 12 ($p < 0.05$) and 24 h ($p < 0.001$). Data derived from three experiments conducted in duplicate.

35
36
37
38
39
40
41
42
43
44
45
46
47
48
49
50
51
52
53
54
55
56
57
58
59
60
61
62
63
64
65

Fig. 7 nanomolar irDE-MPIGA induces externalization of phosphatidylserine in U87MG cells. U87MG cells were treated with irDE-MPIGA (1.25×10^{-3} nmol/ 1×10^6 cells) for indicated times. Harvested cells were stained with annexin V/7-AAD and analyzed by flow cytometry. **A)** Representative dot plots: the lower left quadrant shows the viable cells, the upper left quadrant shows cell debris, the lower right quadrant shows the early apoptotic cells and the upper right quadrant shows the late apoptotic and necrotic cells. The bar graph shows a significant increase of cells in the early phase of apoptosis after 6 h of nanomolar irDE-MPIGA treatment ($p < 0.001$) **(B)** and after 24 of 2.5 μ M PIGA treatment ($p < 0.001$) **(C)**. L= live; EA= early apoptosis; LA= late apoptosis; D= dead.

1
2
3
4
5
6
7
8
9
10
11
12
13
14
15
16
17
18
19
20
21
22
23
24
25
26
27
28
29
30
31
32
33
34
35
36
37
38
39
40
41
42
43
44
45
46
47
48
49
50
51
52
53
54
55
56
57
58
59
60
61
62
63
64
65

Fig. 8 nanomolar irDE-MPIGA affects MPT pore activity in U87MG cells. The U87MG cells were suspended with CRC medium and permeabilized with digitonin. To the CRC-suspended, permeabilized-cells were added 0.25 μM Calcium Green-5N, 5 mM succinate and a train of Ca^{2+} pulses. **A)** Representative traces of U87MG cell treatment with 1 μM CsA or 5 μM CCCP are reported in blue and orange, respectively. Trace black is control sample. **B)** simultaneously to Ca^{2+} loading, permeabilized-cells were incubated with a low nanomolar dose of irDE-MPIGA (1.25×10^{-3} nmol/ 1×10^6 cells) or micromolar dose of PIGA. Representative traces of U87MG cell treatment with irDE-MPIGA or PIGA are reported in red and green, respectively. **C)** In order to reach irreversibility of ligand binding to TSPO, permeabilized-cells were incubated for 2 h with a low nanomolar dose of irDE-MPIGA (1.25×10^{-3} nmol/ 1×10^6 cells) before Ca^{2+} loading. Representative traces of U87MG cell treatment with irDE-MPIGA is reported in red. Trace black is control sample. **D)** Results were represented as CRC normalized to CRC of control (CRC_0). The simultaneous addition of irDE-MPIGA and Ca^{2+} loading in cell suspension significantly increased the CRC ($p < 0.01$). irDE-MPIGA added 2 h before the Ca^{2+} loading was able to reduce the CRC ($p < 0.001$). PIGA, added simultaneously to Ca^{2+} loading, lowered CRC with respect to control sample ($p < 0.05$). Data refer to the mean \pm SEM of three independent experiments.

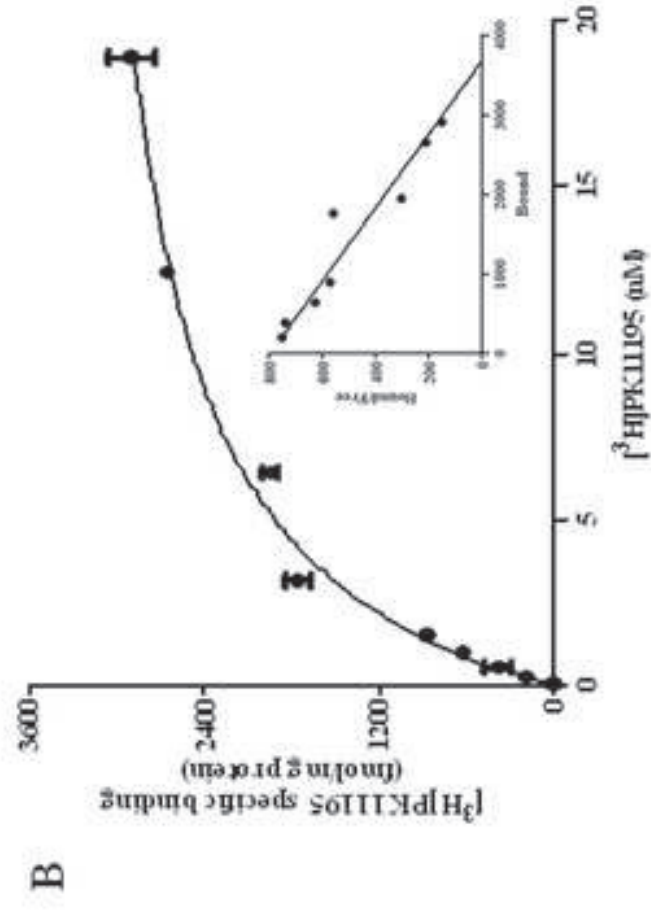
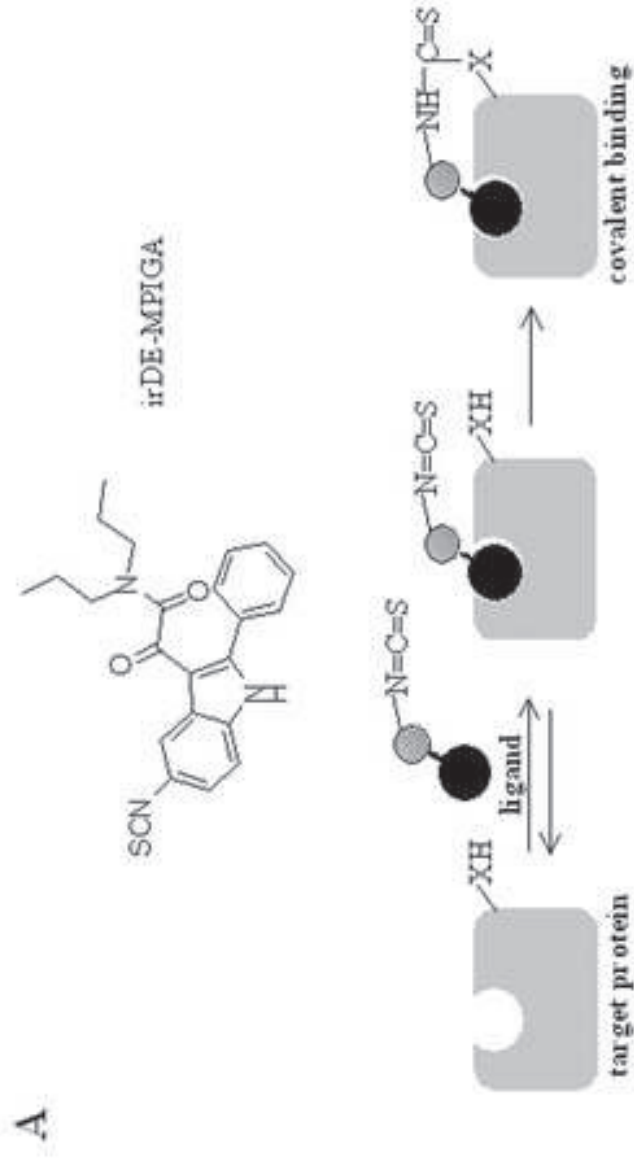


Fig. 1

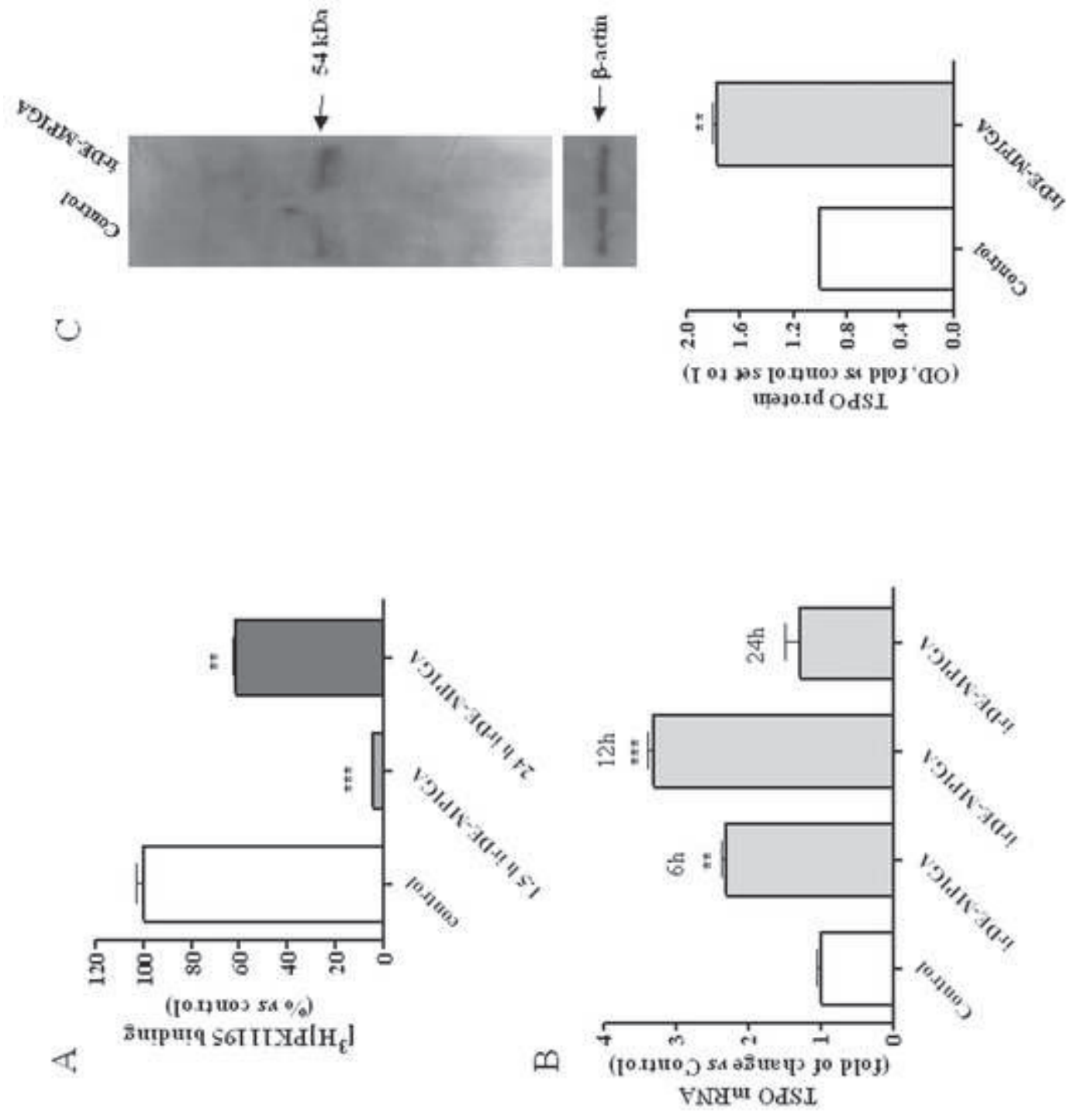


Fig. 2

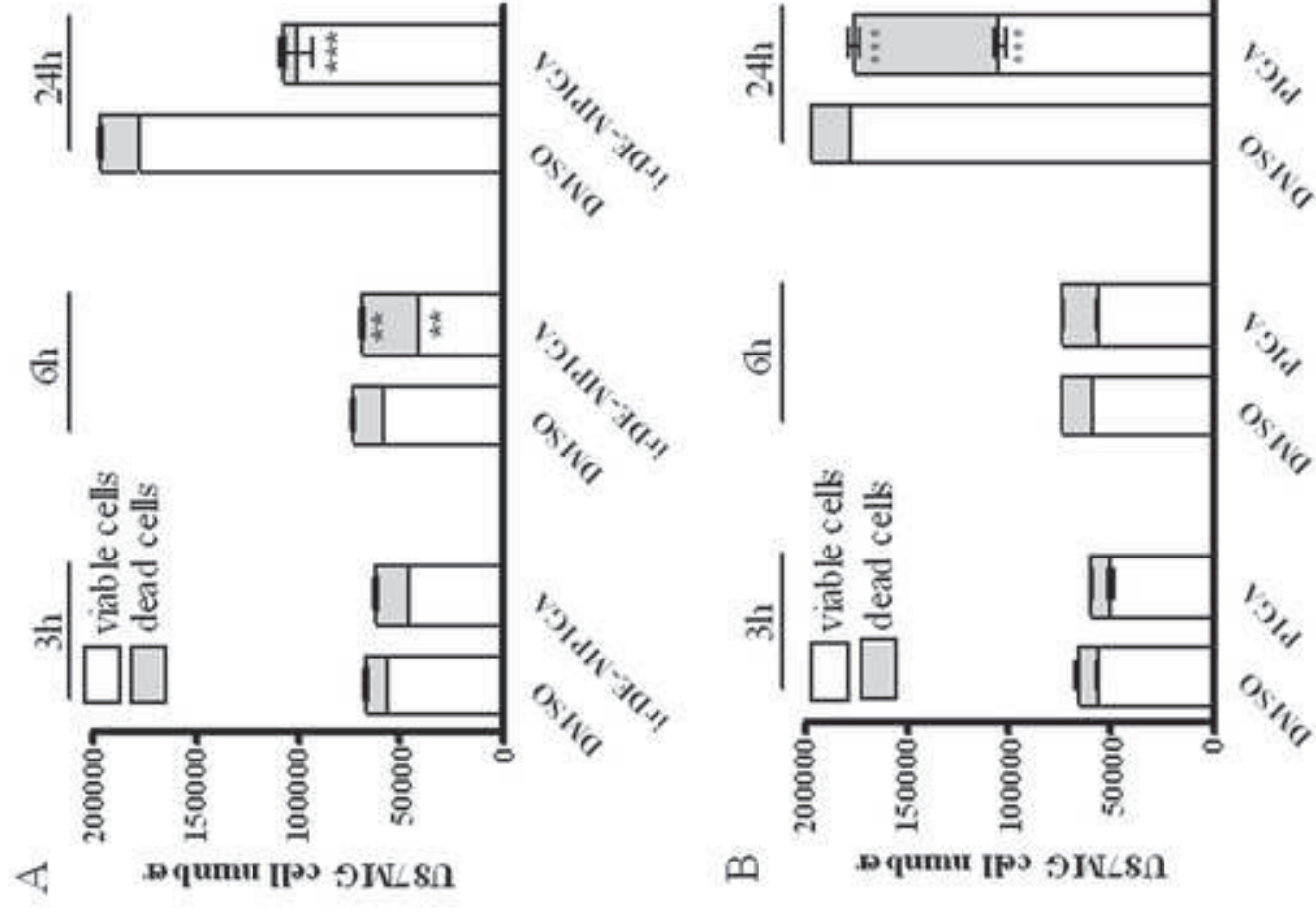


Fig. 3

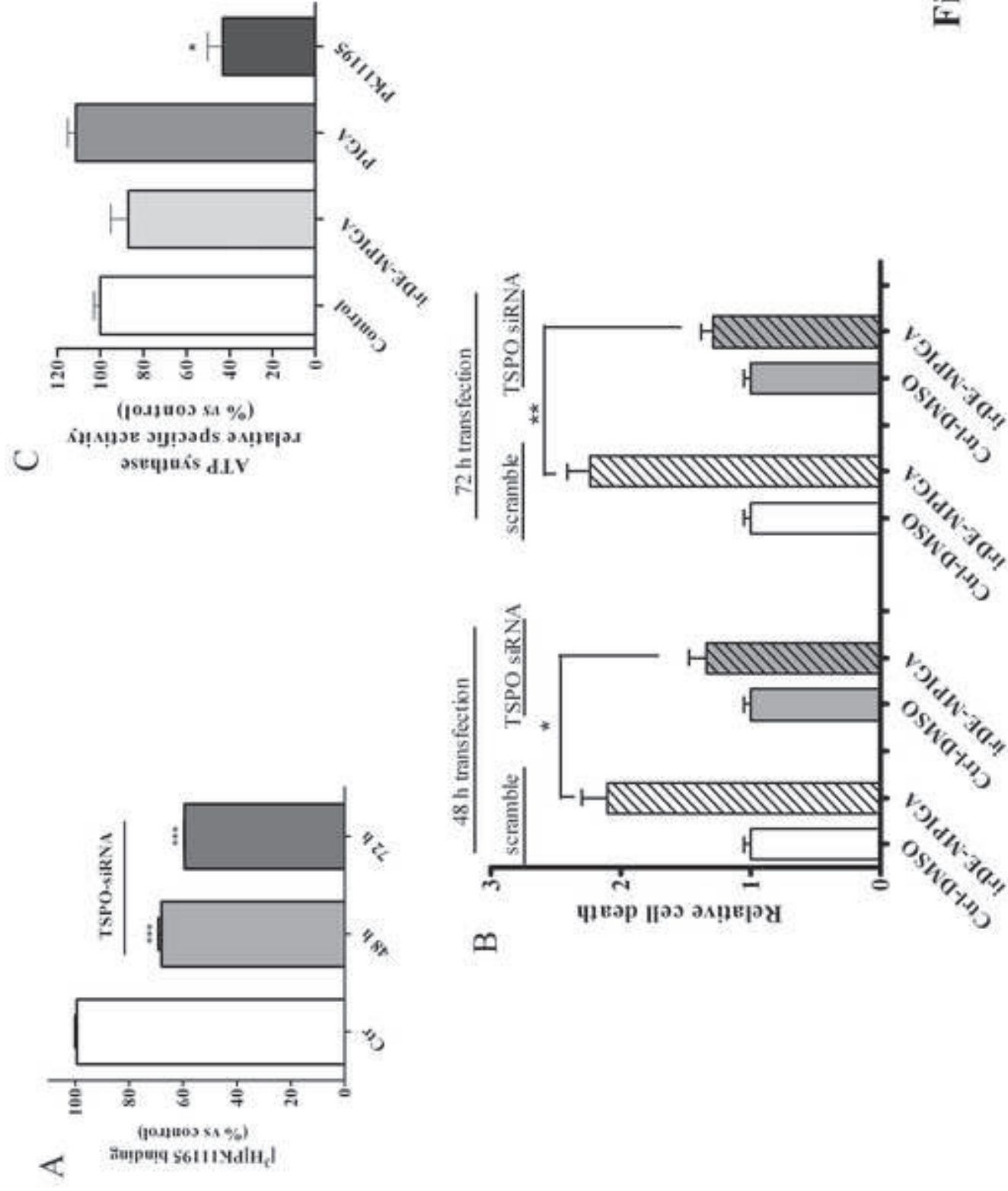


Fig. 4

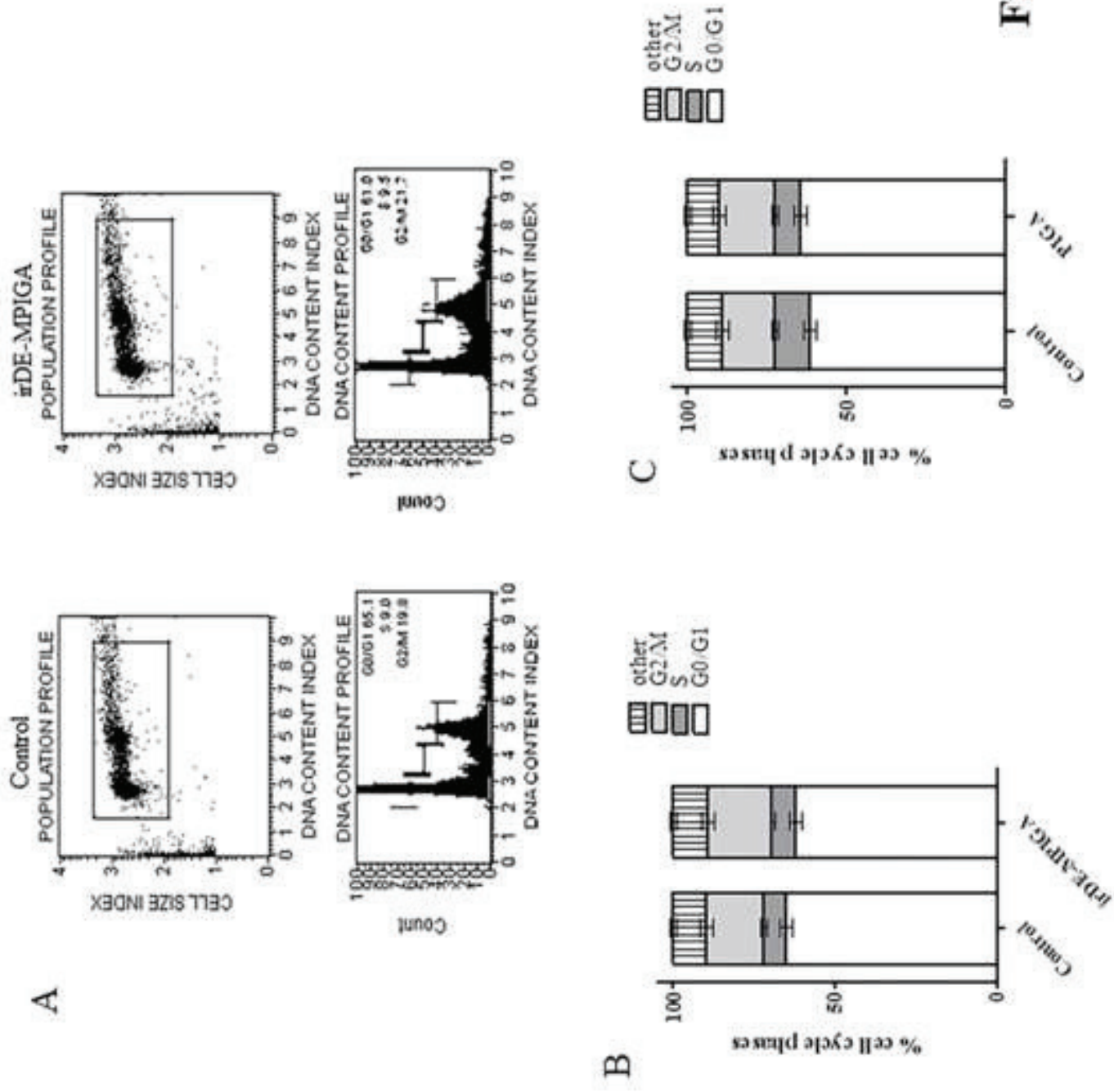


Fig. 5

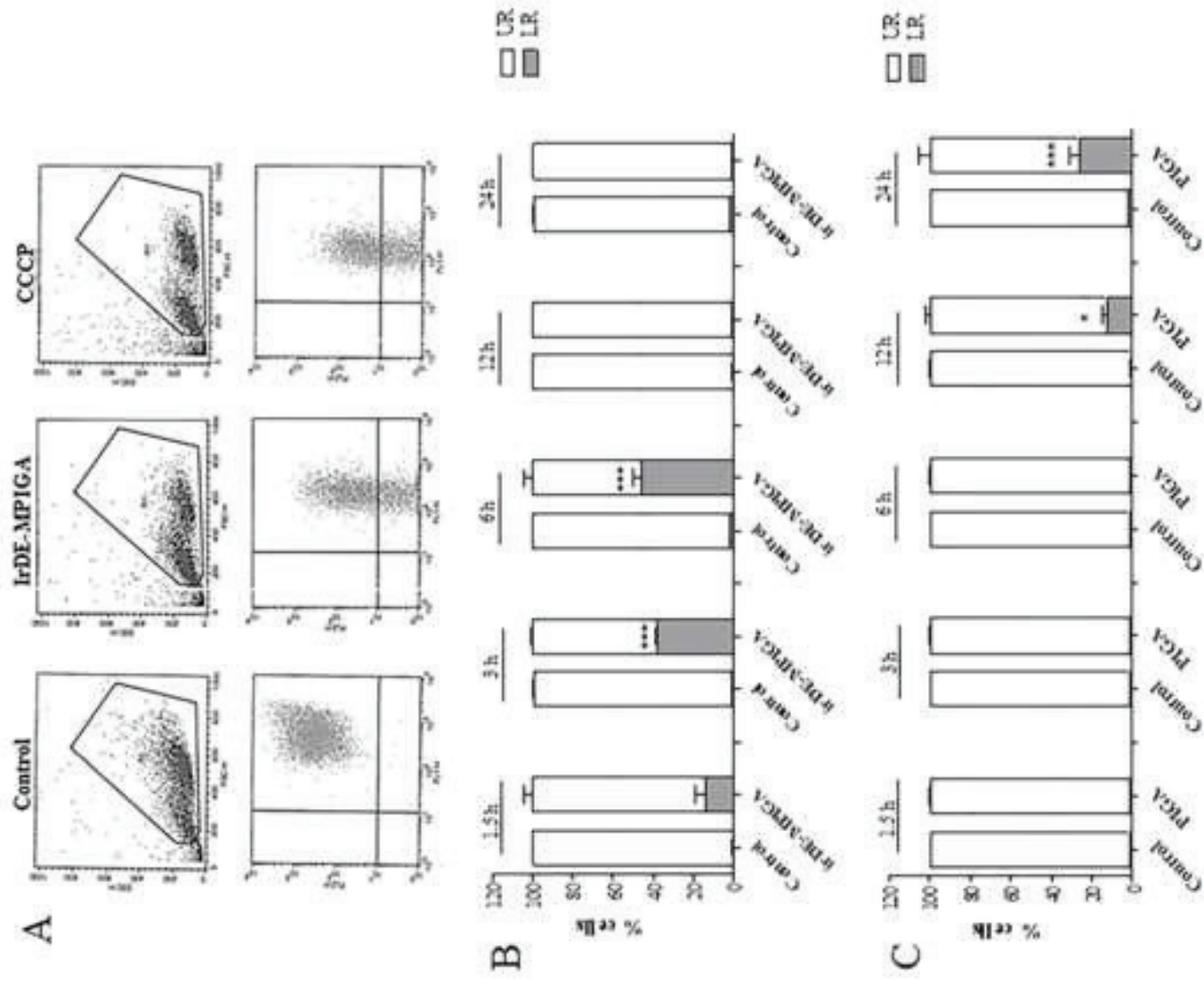


Fig. 6

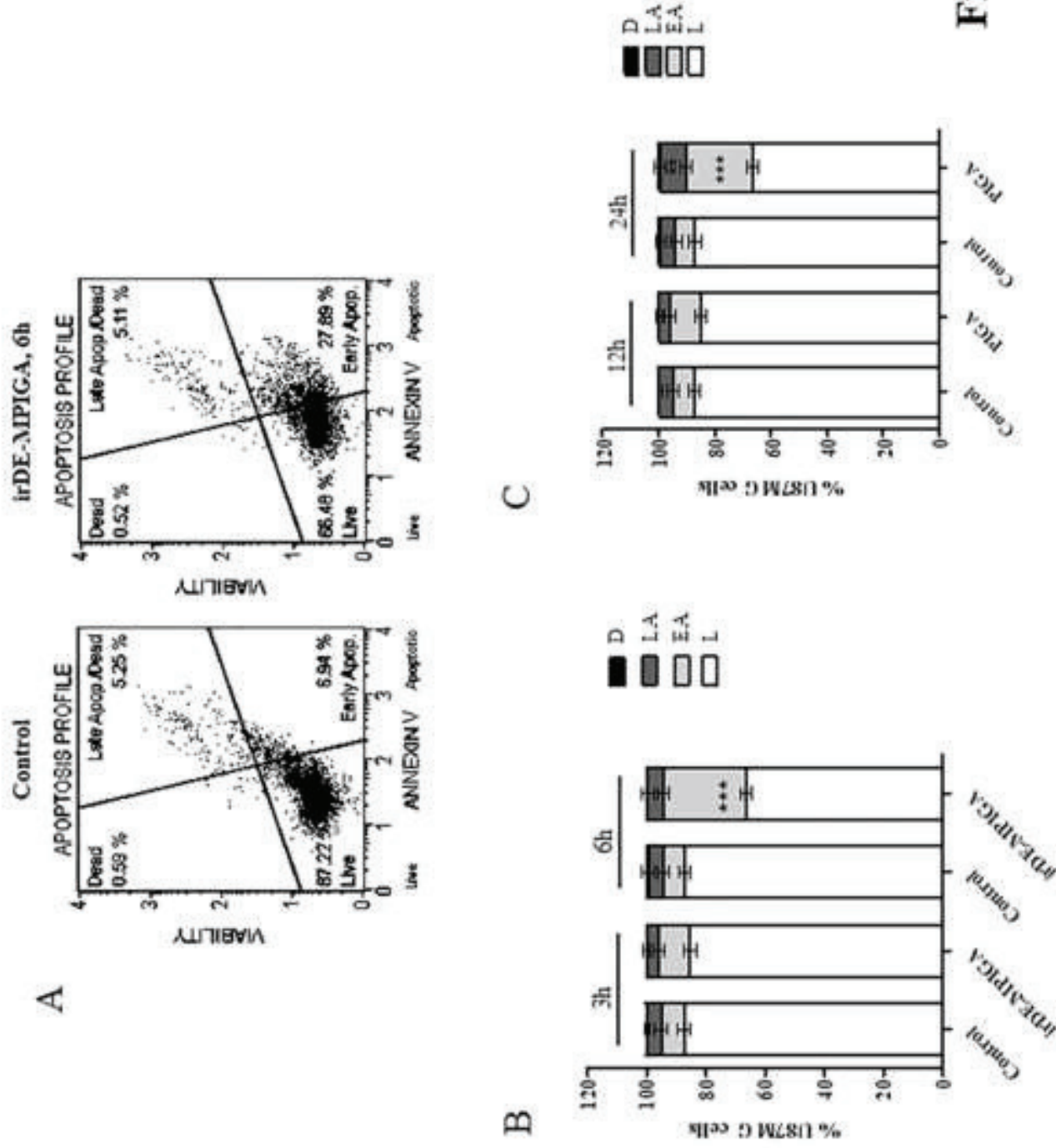


Fig. 7

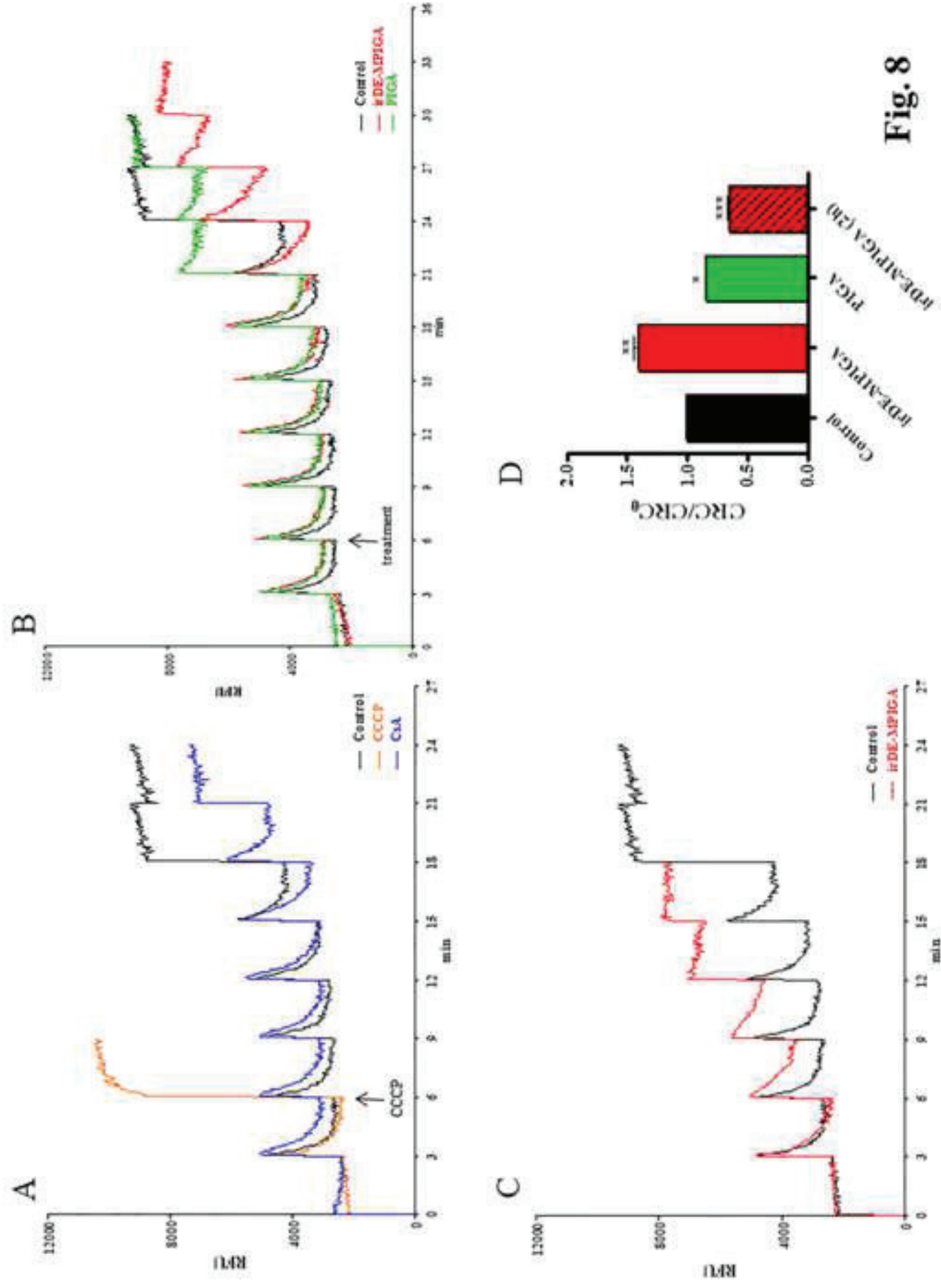


Fig. 8